Chapter 3
Rock Fracture under Static and Dynamic Stress

Jiming Kang, Zheming Zhu and Po Chen

Fracture mechanics is the field of mechanics concerned with the study of the propagation of cracks in materials. It uses methods of analytical solid mechanics to calculate the driving force on a crack and those of experimental solid mechanics to characterize the material's resistance to fracture.As is well known,earthquake happens when energy is released at the fault.Detailed study of active fault show that this model—elastic-rebound theory—applies to most major earthquake.But the stress distribution in the earth crust is so complex that it is still hard for us to get a whole picture of the distribution of earthquake.Recently, fracture mechanics is introduced to earthquake, and becomes an effective method in analyzing the earthquake development and nucleation and redistribution of stress induced by an earthquake.This chapter presents the application of rock fracture mechanics in earthquake and its prediction.A general theory will be given at first,such as three kinds of modes of crack, the stress field near the crack tip and energy release rate, etc.Then we will introduce some recent application of rock fracture mechanics and discuss some challenging issues.

Key words: Fracture mechanics, Sed, Cg, Slip-weakening, Finite element method, Earthquake nucleation, Stress redistribution

3.1 Introduction

Fracture mechanics is an important tool in improving the performance of mechanical components. It applies the physics of stress and strain, in particular the theories of elasticity and plasticity, to the microscopic crystallographic de-

fects found in real materials for predicting the macroscopic mechanical failure of bodies. Fractography is widely used with fracture mechanics to understand the causes of failures and also verify the theoretical failure predictions with real life failures. The prediction of crack growth is a main task of the damage tolerance discipline.

There are three ways of applying a force to enable a crack to propagate (Fig. 3.1):

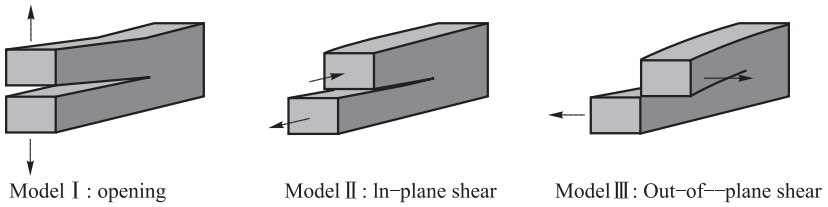

Fig. 3.1 The three modes of fracture.

- Mode I fracture – Opening Mode
- Mode II fracture – Sliding mode
- Mode III fracture – Tearing mode

A fault is a planar fracture or discontinuity in a volume of rock, across which there has been significant displacement along the fractures as a result of the earth movement. Large faults within the Earth's crust result from the action of plate tectonic forces, with the largest forming the boundaries between the plates, such as subduction zones or transform faults. Energy release associated with rapid movement on active faults is the cause of most earthquakes.

Some seismic faults can be considered as cracks and subjected to a compressed stress from environment around it. A simple model is shown in Figure 3.2 (the mixed model of Mode I and Mode II):

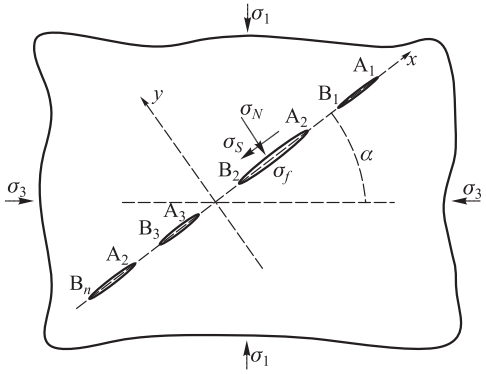

Fig. 3.2 An infinite plane containing a group of collinear cracks under compression, where σ_N is normal stress, σ_S is shear stress.

3.2 Stress Intensity Factor and Stress Field

The stress intensity factor K is used in fracture mechanics to predict the stress state around the tip of a crack caused by a remote load or residual stresses (Griffith, 1921; Irwin, 1957; Erdogan, 2000). It is a theoretical construct usually applied to a homogeneous, linear elastic material, and is useful for providing a failure criterion for brittle materials and a critical technique in the discipline of damage tolerance. The concept can also be applied to materials that exhibit small-scale yielding at a crack tip (Orowan, 1948). The magnitude of K depends on sample geometry, the size and location of the crack, and the magnitude and the modal distribution of loads on the material.

Linear elastic theory predicts that the stress distribution (σ_{ij}) near crack tip, in polar coordinates (r, θ) with origin at the crack tip, has the form (Dugdale, 1960; Barenblatt, 1962; Willis, 1967; Anderson, 1995; Camacho and Ortiz, 1997; Buckley, 2005):

$$\sigma_{ij}(r,\theta) = \frac{K}{\sqrt{2\pi r}} f_{ij}(\theta) + O(r,\theta)$$

where K is the stress intensity factor and f_{ij} is a dimensionless quantity that varies with the load and geometry. This relation breaks down very close to the tip (small r) because as r approaches to 0, the stress σ_{ij} goes to ∞. Thus, plastic distortion occurs at high stresses and the linear elastic solution is no longer applicable close to the crack tip. However, if the crack-tip plastic zone is small, it can be assumed that the stress distribution near the crack is still given by the above relation.

In this chapter, the stress intensity factors for an infinite plane containing collinear cracks (Newman, 1971; Nemat-Nasser and Horii, 1982; Steif, 1984; Ashby and Hallam, 1986; Li and Nordlund, 1993; Germanovich et al., 1994; Baud et al., 1996; Zhu, 1999; Rice et al., 2001; Zhu et al., 1997, 2006) under a far field principal stress σ_1 and σ_3 shown in Figure 3.2 will be studied by using complex stress functions. According to Zhu et al. (1996), for the elastic plane problem, the stress can be expressed in terms of the complex stress functions, Φ and $\Omega(z)$, as

$$\sigma_x + \sigma_y = 2[\Phi(\dot{z}) + \overline{\Phi(z)}] \tag{3.1}$$

$$\sigma_y - i\tau_{xy} = \Phi(z) + \Omega(\bar{z}) + (z - \bar{z})\overline{\Phi'(z)} \tag{3.2}$$

where $z = x + iy$. The equilibrium equations and the compatibility conditions are automatically satisfied, and the resultant force boundary condition can be expressed as

$$i\int_A^B (\overline{X} + i\overline{Y})ds = [\varphi(z) + \omega(\bar{z})\overline{\Phi(z)}]_A^B \tag{3.3}$$

where $\varphi(z) = \int \Phi(z)dz$ and $\omega(z) = \int \Omega(z)dz$, and $\overline{X}, \overline{Y}$ are the surface forces along the boundary in x and y directions, respectively, and A is an arbitrary point on boundary. The positive direction of the integral is assumed that the region always lies to the left. The displacement boundary condition can be expressed as

$$2G(u+iv) = \frac{3-\mu}{1+\mu}\varphi(z) - \omega(\bar{z}) - (z-\bar{z})\overline{\Phi(z)} \tag{3.4}$$

where $G = E/2(1+\mu)$, E is elastic modules and μ is Poisson's ratio. The stress boundary condition can be written as

$$\begin{aligned} \sigma_x l + \tau_{xy} m &= X_n \\ \tau_{xy} l + \sigma_y m &= Y_n \end{aligned} \tag{3.5}$$

where l and m are the direction cosines of the normal line of the boundary, and X_n, Y_n are the force components on the boundary. From equation (3.5) and Fig. 3.2, on the crack surface

$$\begin{aligned} (\sigma_y)^+ &= -\sigma_N, \quad (\tau_{xy})^+ = -\sigma_f \quad \text{(uppersurface)} \\ (\sigma_y)^- &= -\sigma_N, \quad (\tau_{xy})^- = -\sigma_f \quad \text{(lowersurface)} \end{aligned} \tag{3.6}$$

where σ_f and σ_N are the crack surface friction and normal stress, respectively (see Fig. 3.1). Substituting equation (3.6) into (3.2), one can have

$$\begin{aligned} (\sigma_y)^+ - i(\tau_{xy})^+ &= \Phi^+(t) + \Omega^-(t) = -\sigma_N + i\sigma_f \\ (\sigma_y)^- - i(\tau_{xy})^- &= \Phi^-(t) + \Omega^+(t) = -\sigma_N + i\sigma_f \end{aligned} \tag{3.7}$$

or

$$\begin{aligned} [\Phi(t) + \Omega(t)]^+ + [\Phi(t) + \Omega(t)]^- &= -2\sigma_N + 2i\sigma_f = Q \\ [\Phi(t) - \Omega(t)]^+ - [\Phi(t) - \Omega(t)]^- &= 0 \end{aligned} \tag{3.8}$$

where Q is a constant. This is a simple Hilbert problem.

If the shear stress σ_s ($\sigma_s = \frac{\sigma_1-\sigma_3}{2}\sin 2a$), which is parallel to the crack surface, is less than the crack surface fiction, i.e. $\sigma_s < f\sigma_N$, where $\sigma_N = \frac{\sigma_1+\sigma_3}{2} + \frac{\sigma_1-\sigma_3}{2}\cos 2a$, then the crack tip stress intensity factor is zero because large crack surface friction will result in a crack tip without stress concentration, only when $\sigma_s \geqslant f\sigma_N$, the crack tip SIF exists, and in this case σ_f can be written as:

$$\sigma_f = \sigma_N f = \left(\frac{\sigma_1+\sigma_3}{2} + \frac{\sigma_1-\sigma_3}{2}\cos 2a\right) f \tag{3.9}$$

For the problem of multiple cracks shown in Fig 3.2, the Plemelj function can be written as

$$X(z) = 1/\sqrt{(z-a_1)(z-a_2)(z-a_3)\cdots(z-a_n)} \tag{3.10}$$

It can be seen that as $z \to \infty$, $z^n X(z) \to 1$, where n is the number of crack tips. Suppose t_0 is a point on crack surfaces, and if $X(z)$ has a unique limit as $z \to t_0$ along any path in the right neighborhood of t_0, we denote this limit by $X^+(t_0)$. Similarly, if a unique limit exists on approach to t_0 from the left neighborhood, it is denoted by $X^-(t_0)$. In order to investigate the relation between $X^+(t)$ and $X^-(t)$ as $X(z)$ crosses the crack, let's trace a path beginning at a point D on a crack surface and leading from the right side of the crack around the crack tip A_1 to approach D from the left as shown in Figure 3.3. It can be seen that the modulus of all the vectors will not change except for $z - a_8$, and all vectors will increase by 2π in argument whereas the vector $z - a_8$ will return to its original value in argument. Therefore, from equation (3.10), one can have

$$X^-(t) = X^+(t) \cdot \mathrm{e}^{0.5\times(n-1)\times(-2\pi)i} = -X^+(t) \tag{3.11}$$

where n is crack tip number, and for the case in Figure 3.3, $n = 8$.

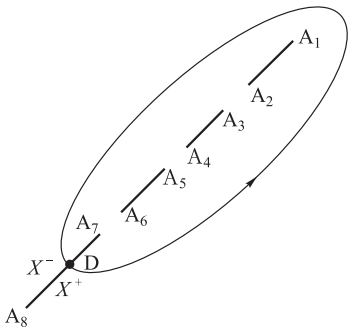

Fig. 3.3 Sketch of a path.

In equation (3.8), $\Phi(t)$ and $\Omega(t)$ are stress complex functions and according to the stress single-valued condition in multi-connected zones, they can be written as

$$\Phi(z) = B - \frac{1+v}{8\pi}(X+iY)\frac{1}{z} + \frac{a_1}{z^2} + \frac{a_2}{z^3} + \cdots \tag{3.12}$$

$$\Omega(z) = B + C - iD + \frac{3-v}{8\pi}(X+iY)\frac{1}{z} + \frac{b_1}{z^2} + \frac{b_2}{z^3} + \cdots \tag{3.13}$$

where v *is* Poisson's ratio, B, C, and D are constants, and they can be determined by the far field principal stresses, i.e.

$$B = \frac{1}{4}(\sigma_1 + \sigma_3)$$

$$C = -\frac{\sigma_1 - \sigma_3}{2}\cos 2\left(\frac{\pi}{2} - \alpha\right) = \frac{\sigma_1 - \sigma_3}{2}\cos 2\alpha$$

$$D = \tau_{xy} = \frac{\sigma_1 - \sigma_3}{2}\sin 2\left(\frac{\pi}{2} - \alpha\right) = \frac{\sigma_1 - \sigma_3}{2}\sin 2\alpha$$

As $z \to \infty$, from equations (3.12) and (3.13), one can have $\Phi(\infty) = B$ and $\Omega(\infty) = B + C - iD$. Let $E(t) = \Phi(t) + \Omega(t)$ and $F(t) = \Phi(t) - \Omega(t)$, equations (3.3) and (3.4) can be rewritten as

$$E^+(t) + E^-(t) = Q(t) \tag{3.14}$$

$$E^+(t) - F^-(t) = 0 \tag{3.15}$$

Equations (3.14) and (3.15) are simple Hilbert problem, and dividing through by $X^+(t)$ and $X^-(t)$, from equation (10), one can have

$$\frac{E^+(t)}{X^+(t)} - \frac{E^-(t)}{X^-(t)} = \frac{Q(t)}{X^+(t)} \tag{3.16}$$

Let $G(t) = \dfrac{E(t)}{X(t)}$ and $g(t) = \dfrac{Q(t)}{X^+(t)}$, then equation (3.16) can be rewritten as

$$G^+(t) - G^-(t) = g(t) \tag{3.17}$$

According to the theory of Cauchy integral on an arc (England, 1971), the general solution of equation (3.17) can be written as

$$G(z) = \frac{1}{2\pi i} \int_L \frac{g(t)dt}{t - z} + P_2(z). \tag{3.18}$$

According to the function's relationship defined above, from equation (3.18), one can have

$$\Phi(z) + \Omega(z) = \frac{X(z)}{2\pi i} \int_L \frac{Q(t)dt}{X^+(t)(t - z)} + X(z)P_2(z) \tag{3.19}$$

Equation (3.10) can be rewritten as

$$F^+(t) = F^-(t) \tag{3.20}$$

This means that the function $F(z)$ is analytic in the entire plane except possibly at infinite where it can at most have a pole. Hence, by Laurent's theorem, $F(z)$ is a polynomial, and considering the condition that as $z \to \infty$, $F(z)$ is limited, then the general solution is

$$F(z) = \Phi(z) - \Omega(z) = \Phi(\infty) - \Omega(\infty) = -C + iD \tag{3.21}$$

From equations (3.19) and (3.21), the two complex stress functions for the case of collinear cracks under compression can be formulated as (see Erdogan, 1962; England, 1971; Horiand Nemat-Nasser, 1982; Gong, 1994; Wang, 1997; Chen et al., 2003).

$$\Phi(z) = \frac{X(z)}{4\pi i} \int_L \frac{Q(t)dt}{X^+(t)(t - z)} + X(z)P_n(z) - \frac{1}{2}(C - iD) \tag{3.22}$$

$$\Omega(z) = \frac{X(z)}{4\pi i} \int_L \frac{Q(t)dt}{X^+(t)(t - z)} + X(z)P_n(z) + \frac{1}{2}(C - iD) \tag{3.23}$$

where

$$P_n(z) = k_0 + k_1 z + k_2 z^2 + \cdots + k_n z^n;$$
$$C - iD = \frac{1}{2}(\sigma_1 - \sigma_3)\mathrm{e}^{-2i\alpha}$$
$$k_{rt} = B + \frac{1}{2}(C - iD) = \frac{1}{4}(\sigma_1 + \sigma_3) + \frac{1}{4}(\sigma_1 - \sigma_3)\mathrm{e}^{-2i\alpha}$$

where $k_0 \to k_{n-1}$ are constants. They will be determined.
In order to get the solution of $\Phi(z)$ and $\Omega(z)$ from equations (3.22) and (3.23), first we have to solve the following equation

$$I(z) = \int_L \frac{Q(t)dt}{X^+(t)(t-z)} \tag{3.24}$$

where $L = L_1 + L_2$ is the union of the two cracks. For each crack, the integrals along Lk in equation (3.24) can be expressed in terms of integral along a lacet C_k surrounding it as shows in Fig. 3.4, and the integral over the lacet can be evaluated by the residue theory. Considering the contour integral around the lacet C_k, one can have

$$\begin{aligned}\int_{C_k} \frac{f(\zeta)d\zeta}{X(\zeta)(\zeta - z)} = &\int_{L_k} \frac{f(t)dt}{X^+(t)(t-z)} + \lim_{\rho\to 0}\int_{|z-b_k|=\rho} \frac{f(\zeta)d\zeta}{X(\zeta)(\zeta - z)} \\ &- \int_{L_k} \frac{f(t)dt}{X^-(t)(t-z)} + \lim_{\rho\to 0}\int_{|z-a_k|=\rho} \frac{f(\zeta)d\zeta}{X(\zeta)(\zeta - z)}\end{aligned} \tag{3.25}$$

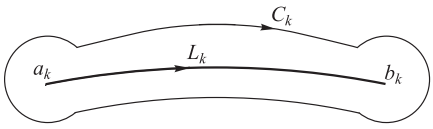

Fig. 3.4 An arc and a lacet surrounding it.

It can be seen that the second and the fourth integrals in equation (3.25) tend to zero as $\rho \to 0$, and combining equation (3.25), one can have

$$\int_{C_k} \frac{f(\zeta)d\zeta}{X(\zeta)(\zeta - z)} = \int_{L_k} \frac{f(t)}{t-z}\left[\frac{1}{X^+(t)} - \frac{1}{X^-(t)}\right]dt = 2\int_{L_k} \frac{f(t)dx}{X^+(t)(t-z)} \tag{3.26}$$

From equation (3.26), the relationship between the integrals along a crack L_k and along its lacet C_k can be obtained

$$I(z) = \int_L \frac{f(t)dt}{X^+(t)(t-z)} = \frac{1}{2}\int_C \frac{f(\zeta)d\zeta}{X(\zeta)(\zeta - z)} \tag{3.27}$$

By using equations (3.27), (3.22) and (3.23) can be rewritten as

$$\Phi(z) = \frac{X(z)}{8\pi i}\int_C \frac{Q(t)dt}{X(t)(t-z)} + X(z)P_n(z) - \frac{1}{2}(C - iD) \tag{3.28}$$

$$\Omega(z) = \frac{X(z)}{8\pi i}\int_C \frac{Q(t)dt}{X(t)(t-z)} + X(z)P_n(z) + \frac{1}{2}(C - iD) \tag{3.29}$$

From the residue theory, the integral in equation (3.27) along contour C can be expressed in terms of the sum of the residues at point z and at infinity, thus equation (3.28) can be rewritten as:

$$\Phi(z) = \frac{QX(z)}{4}\left[\frac{1}{X(z)} + \text{Res}\left(\frac{1}{X(t)(t-z)}, \infty\right)\right] + X(z)P_n(z) - \frac{1}{2}(C - iD) \tag{3.30}$$

In order to determine the coefficient $k_0 \to k_{n-1}$, the conditions of single-valued displacement have to be applied, which can be expressed as

$$\kappa\int_{C_k} \Phi(z)dz - \int_{C_k} \Omega(\bar{z})d\bar{z} = 0 \quad (k = 1, 2\cdot, n) \tag{3.31}$$

where $\kappa = (3-\nu)/(1+\nu)$ for plane stress and $\kappa = 3 - 4\nu$ for plane strain, ν is Poisson's ratio, and C_k is the contour of the kth crack. If the contour C_k shrinks to a lacet around the crack, equation (3.31) can be rewritten as

$$\kappa\int_{L_k} [\Phi^+(t) - \Phi^-(t)]dt - \int_{L_k} [\Omega^-(t) - \Omega^+(t)]dt = 0 \quad (k = 1, 2\cdot, n) \tag{3.32}$$

where t is the coordinates of a point on the crack surface. Applying equation (3.32) for $k = 1, 2, \cdots, n$, one can yield n linear equations, from which the n coefficients can be obtained. Therefore, for an infinite plate containing finite collinear cracks under tension, one may obtain the stress function $\Phi(z)$ and $\Omega(z)$. However, because the stress functions contain the Plemelj function $X(z)$, the process of solving n coefficients maybe difficult due to the high-order integrals involved.

In order to qualitatively investigate the effect of confining stress on SIFs, the corresponding photo-elastic experiment using poly-carbonate (PC) plates is conducted, and the test results are shown in Figure 3.4. The PC plate size is 15cm × 15cm × 0.6cm; the crack length is 1.0 cm; the crack width is 0.1 cm; and the crack orientation is 60°. The vertical stress varies from 0 to 2 MPa. From the photo-elastic results in Figure 3.5, it can be clearly seen that the density of fringes on crack tips increase as the stress increase, indicating that SIF increases as confining stress increases, and therefore, the photo-elastic results qualitatively are in line with the theoretical results.

First, consider a single crack under compression as Figure 3.6

(a) (b) (c)

Fig. 3.5 (See color insert.) The photo-elastic results of the order of fringes for PC plates with confining stress; the parameters: crack lengths are 1.0 cm and 2.0cm , crack tip distance is 1.0 cm, $\alpha = 60°$.

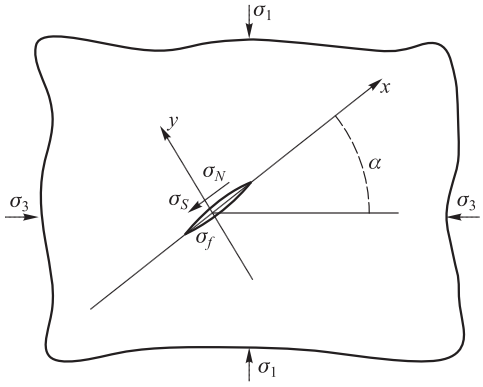

Fig. 3.6 Single crack in infinite plane under compression.

Based on the previous result, for an infinite plane as shown in Figure 3.6, the corresponding function can be simplified as:

$$X(z) = 1/\sqrt{(z^2 - a^2)} \tag{3.33}$$

and the corresponding polynomial $P_n(z) = k_0 + k_1 z$ where $k_1 = k_n$.

In this case, $Q = -2\sigma_N + 2i\sigma_f = (-1 + f)2\sigma_N$ and $\Phi(z)$ can be written as:

$$\Phi(z) = \frac{X(z)}{4\pi i} \int_L \frac{Q(t)dt}{X^+(t)(t - z)} + X(z)P_n - \frac{1}{2}(C - iD) \tag{3.34}$$

$$\Omega(z) = \frac{X(z)}{4\pi i} \int_L \frac{Q(t)dt}{X^+(t)(t - z)} + X(z)P_n + \frac{1}{2}(C - iD) \tag{3.35}$$

Substituting equations (3.34) and (3.35) into equation (3.32), one can have:

$$(2\kappa + 1) \int_{-a}^{a} \frac{k_0 + k_1 z}{X(z)} = 0 \tag{3.36}$$

Because the crack and load is symmetric, $k_0 = 0$ where

$$k_1 = B + \frac{1}{2}(B' - iC') = -\frac{1}{4}(\sigma_1 + \sigma_3) - \frac{1}{4}(\sigma_1 - \sigma_3)\mathrm{e}^{2i\alpha}$$

Thus $\Phi(z)$ can be expressed as:

$$\Phi(z) = X(z)S_0 z + \frac{Q}{4} - \frac{1}{2}(C - iD)$$

where $S_0 = -\frac{Q}{4} + k_1$

$$\Omega(z) = X(z)S_0 z + \frac{Q}{4} + \frac{1}{2}(C - iD)$$

The stress intensity factors (SIFs) can be calculated by

$$\begin{aligned} K_1 - iK_{\mathrm{II}} &= \lim_{z\to a} 2\sqrt{2\pi(z-ct)}\Phi(z) = 2\sqrt{\pi a}\left(-\frac{Q}{4} + k_1\right) \\ &= i\sqrt{\pi a}\left\{f\left[\left(\frac{\sigma_1+\sigma_3}{2}\right) + \left(\frac{\sigma_1-\sigma_3}{2}\right)\sin 2\alpha\right] - \left(\frac{\sigma_1-\sigma_3}{2}\right)\sin 2\alpha\right\} \\ &= -i\sqrt{\pi a}(-f\sigma_N + \sigma_s) \end{aligned}$$

and then

$$K_1 = 0, \quad K_{\mathrm{II}} = \sqrt{\pi a}(-f\sigma_N + \sigma_s) \tag{3.37}$$

where K_1, K_{II} are the SIFs of model I and model II respectively. Because the right part of the equation (3.37) is pure imaginary function, the model I factor K_1 is zero, which means that the K_1 has no impact on the crack or fault under compression. One also can get the stress field at the crack tip as follows:

$$\begin{aligned} \sigma_x &= \frac{K_{\mathrm{II}}}{\sqrt{2\pi r}}\left(-\sin\frac{\theta}{2}\right)\left(2 + \cos\frac{\theta}{2}\cos\frac{3\theta}{2}\right) \\ \sigma_y &= \frac{K_{\mathrm{II}}}{\sqrt{2\pi r}}\sin\frac{\theta}{2}\cos\frac{\theta}{2}\cos\frac{3\theta}{2} \\ \tau_{xy} &= \frac{K_{\mathrm{II}}}{\sqrt{2\pi r}}\cos\frac{\theta}{2}\left(1 - \sin\frac{\theta}{2}\sin\frac{3\theta}{2}\right) \end{aligned}$$

or

$$\begin{aligned} \sigma_{rr} &= \frac{K_{\mathrm{II}}}{\sqrt{2\pi r}}\sin\frac{\theta}{2}\left(1 - 3\sin^2\frac{\theta}{2}\right) \\ \sigma_{\theta\theta} &= \frac{K_{\mathrm{II}}}{\sqrt{2\pi r}}\left(-3\sin\frac{\theta}{2}\cos^2\frac{\theta}{2}\right) \\ \tau_{r\theta} &= \frac{K_{\mathrm{II}}}{\sqrt{2\pi r}}\left(1 - 3\sin^2\frac{\theta}{2}\right) \end{aligned}$$

In order to get more precise stress field, a new coordinate system (see Fig.3.7) should be introduced as below

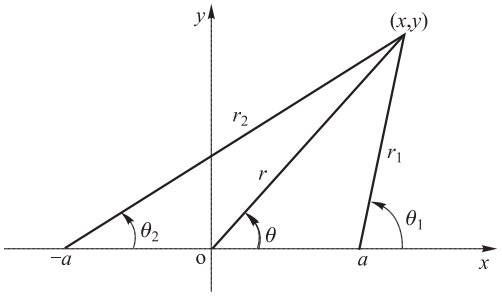

Fig. 3.7 Polar coordinate with r_1, r_2 and θ_1, θ_2.

The Westergaard Stress Function is given for the sake of simplicity:

$$Z_{\mathrm{II}} = \left(\frac{z}{\sqrt{z^2 - a^2}} - 1 \right) \tau^{\infty} \tag{3.38}$$

where $z = re^{i\theta}$, $z - a = r_1 e^{i\theta_1}$, $z + a = r_2 e^{i\theta_2}$, and then equation (3.38) can be written as

$$Z_{\mathrm{II}} = \left[\frac{r}{\sqrt{r_1 r_2}} \mathrm{e}^{i\left(\theta - \frac{\theta_1 + \theta_2}{2}\right)} - 1 \right] \tau^{\infty} \tag{3.39}$$

The derivative of Z_{II} with respect to z is

$$Z'_{\mathrm{II}} = \frac{-a^2 \tau^{\infty}}{(z^2 - a^2)^{3/2}} = \frac{-a^2 \tau^{\infty}}{(r_1 r_2)^{3/2}} \mathrm{e}^{-i\frac{3}{2}\left(\frac{\theta_1 + \theta_2}{2}\right)} \tag{3.40}$$

and the calculus of is

$$\widetilde{Z}_{\mathrm{II}} = \tau^{\infty} \left(\sqrt{z^2 - a^2} - z \right) = \tau^{\infty} \left(\sqrt{(r_1 r_2)} \mathrm{e}^{i\frac{1}{2}\left(\frac{\theta_1 + \theta_2}{2}\right)} - re^{i\theta} \right)$$

So the stress components can be given:

$$\begin{aligned} \frac{\sigma_x + \sigma_y}{2} &= \mathrm{Im} Z_{\mathrm{II}} \\ \frac{\sigma_x - \sigma_y}{2} &= \mathrm{Im} Z_{\mathrm{II}} + y \mathrm{Re} Z'_{\mathrm{II}} \\ \tau_{xy} &= \mathrm{Re} Z_{\mathrm{II}} - y \mathrm{Im} Z'_{\mathrm{II}} \end{aligned} \tag{3.41}$$

Substituting equations (3.39) and (3.40) into equation (3.41), one can have

$$\begin{aligned} \frac{\sigma_x + \sigma_y}{2} &= \frac{r\tau^{\infty}}{\sqrt{r_1 r_2}} \sin\left(\theta - \frac{\theta_1 + \theta_2}{2} \right) \\ \frac{\sigma_x - \sigma_y}{2} &= \tau^{\infty} \left[\frac{r}{\sqrt{r_1 r_2}} \sin\left(\theta - \frac{\theta_1 + \theta_2}{2} \right) - \frac{a^2 r}{(r_1 r_2)^{3/2}} \sin\theta \cos\frac{3(\theta_1 + \theta_2)}{2} \right] \\ \tau_{xy} &= \tau^{\infty} \left\{ \left[\frac{r}{\sqrt{r_1 r_2}} \cos\left(\theta - \frac{\theta_1 + \theta_2}{2} \right) - 1 \right] \right. \\ &\quad \left. - \frac{a^2 r}{(r_1 r_2)^{3/2}} \sin\theta \sin\frac{3(\theta_1 + \theta_2)}{2} \right\} \end{aligned} \tag{3.42}$$

Also the displacement field can be given by

$$2\mu u = \frac{2\mu}{E'}\mathrm{Im}\widetilde{Z}_{\mathrm{II}} + y\mathrm{Re}Z_{\mathrm{II}}$$
$$2\mu\nu = -\frac{2\mu(1-\nu)}{E'}\mathrm{Re}\widetilde{Z}_{\mathrm{II}} - y\mathrm{Im}Z_{\mathrm{II}}$$

Substituting equations (3.29) and (3.40) into equation (3.42), one can have:

$$\begin{aligned} 2\mu u &= \left\{\frac{4\mu}{E'}\left[\sqrt{r_1 r_2}\sin\left(\tfrac{\theta_1+\theta_2}{2}\right) - r\sin\theta\right] + r\sin\theta\left[\cos\left(\theta - \frac{\theta_1+\theta_2}{2}\right) - 1\right]\right\}\tau^{\infty} \\ 2\mu\nu &= \left\{\frac{2\mu(1\nu)}{E'}\left[\sqrt{r_1 r_2}\cos\left(\tfrac{\theta_1+\theta_2}{2}\right) - r\sin\theta\right] + r\sin\theta\left[\sin\left(\theta - \frac{\theta_1+\theta_2}{2}\right)\right]\right\}\tau^{\infty} \end{aligned} \tag{3.43}$$

When $y = 0$ and $|x| < a$, the displacements on the upper and bottom crack surfaces can be written as:

$$u^{+} = \frac{2\tau^{\infty}}{E'}\sqrt{a^2 - x^2}$$
$$\nu^{+} = \frac{(1-\nu')\tau^{\infty}}{E'}x$$
$$u^{-} = -\frac{2\tau^{\infty}}{E'}\sqrt{a^2 - x^2}$$
$$\nu^{-} = \frac{(1-\nu')\tau^{\infty}}{E'}x$$

Thus,

$$\begin{aligned} \Delta u &= \tfrac{4\tau^{\infty}}{E'}\sqrt{a^2 - x^2} \\ \Delta\nu &= 0 \end{aligned} \tag{3.44}$$

3.3 Coulomb-Mohr Failure Criterion

In the above analyses, we show that the crack surface frictions, confining stresses and distances between two crack tips can affect the stress intensity factors significantly, and thus they affect fault fracture behavior. It is well known that the crack propagation criterion for mode II crack can be written as (Muskelishvili, 1953; Nemat-Nasser and Horii, 1982; Kachanov, 1987; Ballarini and Plesha, 1987; Wang, 1997; Eberhardt and Kim, 1998; Lauterbach and Gross, 1998; Chen, 2003; Fan, 2003; Li et al., 2003; Zhu et al., 2006; Millwater, 2010; Jin, 2013)

$$K_{\mathrm{II}} \leqslant K_{\mathrm{II}C} \tag{3.45}$$

where $K_{\mathrm{II}C}$ is material fracture toughness. The crack propagation criterion in equation (3.45) is difficult to apply because the fracture toughness is generally

difficult to measure. The technique used in measuring material fracture toughness is not flawless, and the measurement results are usually scattered in a large range, especially for brittle materials. In order to avoid such difficulties in measuring material fracture toughness, equation (3.29) will be transformed into a new form expressed in terms of principal stresses, without K_{II} and $K_{\mathrm{II}C}$ involved.

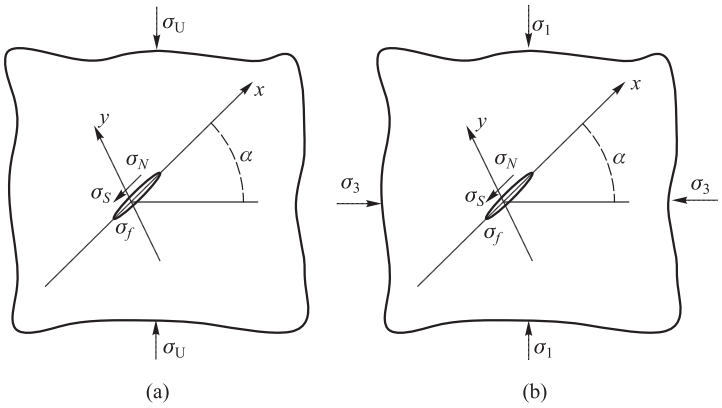

Fig. 3.8 A specimen containing two inclined cracks under (a) uni-axial compression and (b) bi-axial Compression.

Considering a specimen containing two cracks under uni-axial compression as shown in Figure 3.8a, its critical stress is σ_U, and the corresponding K_{II} can be obtained from equation (3.37) by substituting σ_f from equation (3.9) and taking $\sigma_3 = 0$:

$$K_{\mathrm{II}}^U = \sqrt{\pi a}\left(-f\frac{\sigma_U(1+\cos 2\alpha)}{2} + \frac{\sigma_U \sin 2\alpha}{2}\right) \tag{3.46}$$

Under the critical condition, the relation between K_{II} and $K_{\mathrm{II}C}$ can be written as

$$K_{\mathrm{II}} = K_{\mathrm{II}C} \tag{3.47}$$

Substituting equation (3.46) into equation (3.47), we have

$$K_{\mathrm{II}}^U = \sqrt{\pi a}\left(-f\frac{\sigma_U(1+\cos 2\alpha)}{2} + \frac{\sigma_U \sin 2\alpha}{2}\right) = K_{\mathrm{II}C} \tag{3.48}$$

When the confining stress is applied on this specimen as shown in Figure 3.8b, its critical stress will increase from σ_U to σ_1. The corresponding K_{II} can be written as

$$K_{\mathrm{II}} = \sqrt{\pi a}\left(-f\left[\frac{(\sigma_1+\sigma_3)}{2} + \frac{(\sigma_1-\sigma_3)\cos 2\alpha}{2}\right] + \frac{(\sigma_1+\sigma_3)}{2}\sin 2\alpha\right) \tag{3.49}$$

Substituting equations (3.48) and (3.49) into equation (3.47), one can have

$$f(\sigma_1+\sigma_3) + (\sigma_1-\sigma_3)(f\cos\alpha - \sin\alpha) \leqslant \sigma_U(f + f\cos\alpha - \sin\alpha) \tag{3.50}$$

From equation (3.50), the crack propagation criterion for single crack under compression is obtained (Steif, 1984; Ashby and Hallam, 1986; Basista and Gross, 2000)

$$\sigma_1 \leqslant \sigma_U + \frac{1 + f\tan\alpha}{1 - f\tan\alpha}\sigma_3 \tag{3.51}$$

Equation (3.51), known as Coulomb-Mohr failure criterion, is an alternative form of crack propagation criterion for single crack under compression, derived from the general crack propagation criterion, equation (3.35). This criterion is expressed in terms of principal stresses, without K_{II} and $K_{\mathrm{II}C}$ being involved, which is more convenient in application. The critical stress σ_1 in equation (3.41) is related to four parameters: confining stress σ_3, uni-axial compression strength σ_U, crack orientation α, and crack surface friction coefficient f.

Under the critical state, the relation between σ_1 and σ_3 from equation (3.51) can be written as (Erdogan, 1962; England, 1971; Olver et al., 2010)

$$\sigma_1 = \sigma_U + \frac{1 + f\tan\alpha}{1 - f\tan\alpha}\sigma_3$$

It should be noted that the shear stress σ_S in Figure 3.6, which is parallel to the crack surface, must be larger than the crack surface friction $f\sigma_N$, i.e.

$$\frac{(\sigma_1 - \sigma_3)}{2}\sin 2\alpha > f\left[\frac{(\sigma_1 + \sigma_3)}{2} + \frac{(\sigma_1 - \sigma_3)\cos 2\alpha}{2}\right]$$

Otherwise, the SIF is zero due to a large crack surface friction and then the above equation can be rewritten as

$$\frac{\sigma_3}{\sigma_1} = \frac{1 - f\tan\alpha}{1 + f\tan\alpha} \tag{3.52}$$

Therefore, before applying equations (3.49), one should use equation (3.52) to examine if the crack SIF is zero, and if equation (3.52) is not satisfied, the crack tip SIF is zero.

Because $\dfrac{\sigma_3}{\sigma_1} > 0$, from equation (3.52), one can have $1 - f\tan\alpha > 0$, or $\tan\alpha > f$

This means that $\tan\alpha$ should be larger than crack surface friction coefficient f. Otherwise, the corresponding crack SIF must be zero.

3.4 Energy Release and J-integral

3.4.1 Energy Release Rate

The strain energy release rate is the energy dissipated during fracture per unit of newly created fracture surface area. This quantity is central to fracture me-

chanics because the energy that must be supplied to a crack tip for it to grow must be balanced by the amount of energy dissipated due to the formation of new surfaces and other dissipative processes such as plasticity.

For the purposes of calculation, the energy release rate is defined as

$$G = -\frac{\partial(U - W)}{\partial A} \tag{3.53}$$

where U is the potential energy available for crack growth, W is the work associated with any external forces acting, and A is the crack area (crack length for two-dimensional problems). The unit of G is $\mathrm{J/m^2}$.

The energy release rate failure criterion states that a crack will grow when the available energy release rate G is greater than or equal to a critical value G_c, $G \geqslant G_c$ where G_c is the fracture energy and is considered to be a material property which is independent of the applied loads and the geometry of the body.

For two-dimensional problems (plane stress, plane strain, anti-plane shear) involving cracks that move in a straight path, the mode I stress intensity factor K_{I} is related to the energy release rate (G) by $G = \frac{K_{\mathrm{I}}^2}{E'}$ where E is the Young's modulus and $E' = E$ for plane stress and $E' = \frac{E}{(1-\mu^2)}$ for plane strain.

3.4.2 J-integral

The J-integral represents a way to calculate the strain energy release rate, or work (energy) per unit fracture surface area, in a material (Van Vliet, 2006). The theoretical concept of J-integral was developed by Cherepanovn (1967) and by Rice (1968) independently, who showed that an energetic contour path integral was independent of the path.

Later, experimental methods were developed to measure the critical fracture properties using laboratory-scale specimens for materials in which sample sizes are too small and for which the assumptions of Linear Elastic Fracture Mechanics (LEFM) do not hold (Lee and Donovan,. 1987), and to infer a critical value of fracture energy J_κ. The quantity J_κ defines the point at which large-scale plastic yielding during propagation takes place under mode one loading (Rice, 1968).

The J-integral is equal to the strain energy release rate for a crack in a body subjected to monotonic loading (Lee and Donovan, 1987). This is generally true, under quasi-static conditions, only for linear elastic materials. For materials that experience small-scale yielding at the crack tip, J can be used to compute the energy release rate under special circumstances such as monotonic loading in mode III (anti-plane shear). The strain energy release rate can also be computed from J for pure power-law hardening plastic materials that undergo small-scale yielding at the crack tip.

The quantity J is not path-independent for monotonic mode I and mode II loadings of elastic-plastic materials, so only a contour very close to the crack tip gives the energy release rate. Also, Rice shows that J is path-independent in plastic materials when there is no non-proportional loading. Unloading is a special case of this, but non-proportional plastic loading also invalidates the path-independence. Such non-proportional loading is the reason for the path-dependence for the in-plane loading modes on elastic-plastic materials.

The two-dimensional J-integral was originally defined as (*see* Fig. 3.9)

$$J = \int_{\Gamma} \left(w dx_2 - \boldsymbol{t} \cdot \frac{\partial \boldsymbol{u}}{\partial x_1} ds \right) = \int_{\Gamma} \left(w dx_2 - t_i \frac{\partial u_i}{\partial x_1} ds \right) \tag{3.54}$$

where $w(x_1, x_2)$ is the strain energy density, x_1, x_2 are the coordinate directions, $t = n \cdot \sigma$ is the surface traction vector, n is the normal to the curve Γ, σ is the Cauchy stress tensor, and u is the displacement vector.

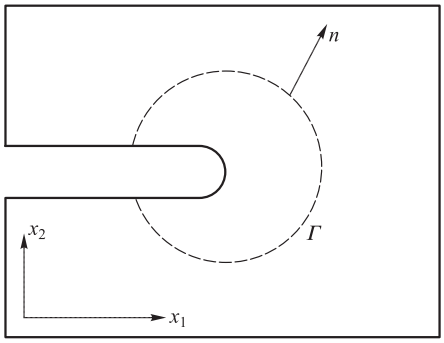

Fig. 3.9 Line J-integral around a notch

For Mode II crack under shear stress τ on the surface, we can have the conservative expression (*see* Fig. 3.10)

$$J_Q + J_{Q^+P^+} - J_P + J_{P^-Q^-} = 0 \tag{3.55}$$

where J_Q is a J-integral along the closure from the bottom surface point Q^- to the upper surface point Q^+. $J_{Q^+P^+}$ is a J-integral along the line from the upper surface point Q^+ to the surface point P^+ (*see* Fig. 3.10).

Equation (3.55) can be rewritten as

$$J_Q + \int_Q^0 \sigma \left(\frac{\partial \delta}{\partial x_1} \right) dx_1 = J_P + \int_P^0 \sigma \left(\frac{\partial \delta}{\partial x_1} \right) dx_1 \tag{3.56}$$

When P is close to the crack tip O, and equation (3.56) has

$$J_Q + \int_Q^0 \sigma \left(\frac{\partial \delta}{\partial x_1} \right) dx_1 = \lim_{P \to O} J_P = G \tag{3.57}$$

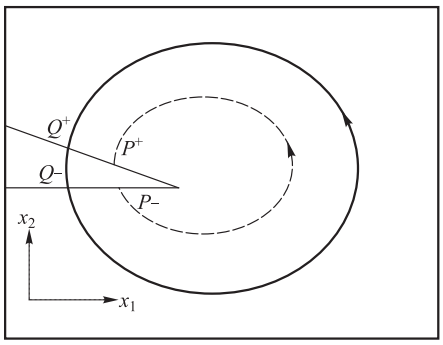

Fig. 3.10 J-integral for the Mode II crack.

For the crack surface under uniform shear stress τ_s, equation (3.57) can be simplified as

$$G = J_Q - \tau_s \delta_Q \tag{3.58}$$

Rice (1968) also showed that the value of the J-integral represents the energy release rate for planar crack growth. The J-integral was developed because of the difficulties involved in computing the stress close to a crack in a nonlinear elastic or elastic-plastic material. Rice showed that if monotonic loading was assumed (without any plastic unloading) then the J-integral could be used to compute the energy release rate of plastic materials too.

For isotropic, perfectly brittle and linear elastic materials, the J-integral can be directly related to the fracture toughness if the crack extends straight ahead with respect to its original orientation (Ramberg et al., 1943; Hutchinson, 1968; Rice, 1968; Rosengren, 1968; Yoda, 1980; Meyers and Chawla; 1999).

Under Mode I loading conditions, this relation is

$$J_{IC} = G_{IC} = \frac{K_{IC}^2}{E'}$$

where G_{IC} is the critical strain energy release rate, J_{IC} is the fracture toughness, and E is the Young's modulus and $E' = E$ for plane stress and $E' = E/(1-\mu^2)$ for plane strain.

For Mode II loading, the relation between the J-integral and the mode II fracture toughness K_{IIC} is

$$J_{IIC} = G_{IIC} = \frac{K_{IIC}^2}{E'}$$

For Mode III loading, the relation is

$$J_{IIIC} = G_{IIIC} = K_{IIIC}^2 \left(\frac{1+\mu}{E}\right)$$

3.5 Crack Growth

Crack criterion is an important problem, which is needed to research from micro, sub-micro and macro views. As an integral crack criterion, it should be able to solve two problems:

1. In which condition will crack initial and continue?
2. In which direction will crack extend?

The research on the rock fracturing mechanism can be traced back to the theory of Griffith brittle fracture model , which means that the crack can't extend until the release rate of the strain energy is larger than the crack surface energy. Later, Irwin introduced SIF—known as K criterion—as crack criterion based on Griffith brittle fracture model. But K criterion cannot answer the problem of the crack with mixed model containing Model I and Model II, so a series of new crack criterion are developed.

3.5.1 Maximum Hoop Stress Theory

Erdogan and Sih (1968) raised the theory when they found that the mixed-model crack extended along the surface that was perpendicular to the maximum hoop stress. In the 2-D model, which means K_{III} is zero, the stress field on the crack tip is shown below:

$$\begin{aligned}
\sigma_{rr} &= \frac{1}{2\sqrt{2\pi r}}\left[K_{\mathrm{I}}\cos\frac{\theta}{2}(3-\cos\theta)+K_{\mathrm{II}}\sin\frac{\theta}{2}(3\cos\theta-1)\right]\\
\sigma_{\theta\theta} &= \frac{1}{2\sqrt{2\pi r}}\cos\frac{\theta}{2}[K_{\mathrm{I}}(1+\cos\theta)-3K_{\mathrm{II}}\sin\theta] \qquad (3.59)\\
\sigma_{r\theta} &= \frac{1}{2\sqrt{2\pi r}}\cos\frac{\theta}{2}[K_{\mathrm{I}}\sin\theta-K_{\mathrm{II}}(3\cos\theta-1)]
\end{aligned}$$

According to the following theory:

Crack extends along the angle which have the max hoop stress $\sigma_{\theta\theta}$, and the direction satisfies

$$\frac{\partial\sigma_{\theta\theta}}{\partial\theta}=0, \quad \frac{\partial^2\sigma_{\theta\theta}}{\partial^2\theta}<0 \qquad (3.60)$$

Substituting the left part in equation (3.54) with the derivative of $\sigma_{\theta\theta}$ with respect to θ in equation (3.59), one can have

$$\cos\frac{\theta}{2}[K_{\mathrm{I}}\sin\theta-K_{\mathrm{II}}(3\cos\theta-1)]=0$$

So that the breaking angle is decided by

$$K_{\mathrm{I}}\sin\theta-K_{\mathrm{II}}(3\cos\theta-1)=0 \qquad (3.61)$$

By comparing the equation (3.61) with the third part in equation (3.59), one can find that $\sigma_{r\theta} = 0$ at the plane of stress of $\sigma_{\theta\theta\,\max}$, which mean the plane is a principle plane of stress.

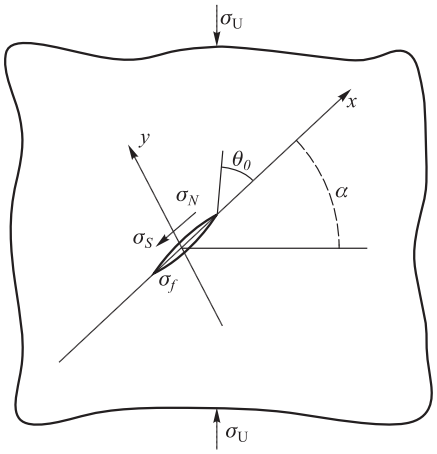

Fig. 3.11 Breaking angle θ_0.

θ_0 is decided by $K_{\rm II}/K_{\rm I}$. When $K_{\rm II} = 0$ (pure Model I), $\theta_0 = 0$, which means the crack develops along itself. But when $K_{\rm II} \neq 0$ and is small, θ_0 increases sharply.

When $K_{\rm I} = 0$ (pure Model II) or $K_{\rm II}/K_{\rm I} \to \infty$,

$$\theta_0 = \text{arcoos}\frac{1}{3} = -70.32^\circ \tag{3.62}$$

When $K_{\rm I} \neq 0$ and $K_{\rm II} \neq 0$,

$$\theta_0 = 2\text{arctan}\frac{[K_{\rm I}/K_{\rm II} \pm \sqrt{(K_{\rm I}/K_{\rm II})^2 + 8}]}{4} \tag{3.63}$$

Figure 3.12 shows the relationship between θ_0 and $K_{\rm II}/K_{\rm I}$.

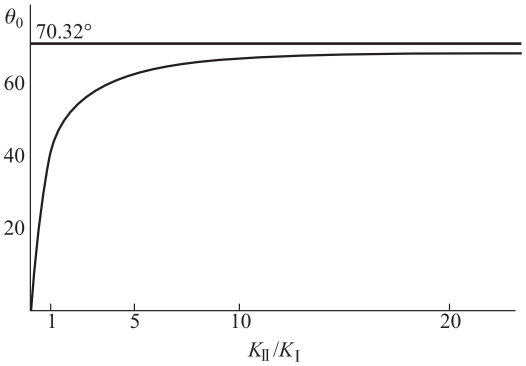

Fig. 3.12 θ_0 versus $K_{\rm II}/K_{\rm I}$.

For the mixed model of crack under a uni-axial stress σ_1 (*see* Fig.3.13).

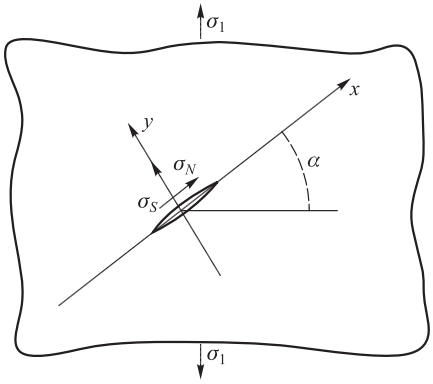

Fig. 3.13 Crack under a uni-axial stress σ_1.

The remote stress σ_N and σ_S is shown below:

$$\sigma_N = \sigma_1 \sin^2 \alpha,\ \sigma_S = \sigma_1 \cos\alpha \sin\alpha,$$

,

So

$$K_{\mathrm{I}} = \sigma\sqrt{\pi a}\sin^2\alpha,\ K_{\mathrm{II}} = \sigma\sqrt{\pi a}\cos\alpha\sin\alpha \tag{3.64}$$

Substituting equation (3.64) into equation (3.61), then the relationship between crack angel α and breaking angle θ is $\sin\theta - (3\cos\theta - 1)\arctan\alpha = 0$.

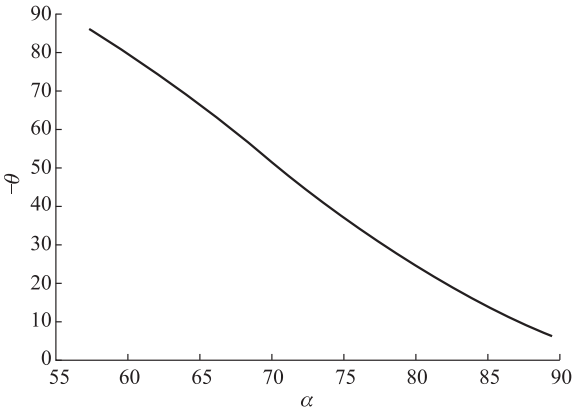

Fig. 3.14 The relationship between crack angel and breaking angle θ.

In order to qualitatively investigate breaking angle, the corresponding experiment using acrylic-material plates is conducted, and the test results are shown in Figure 3.15.

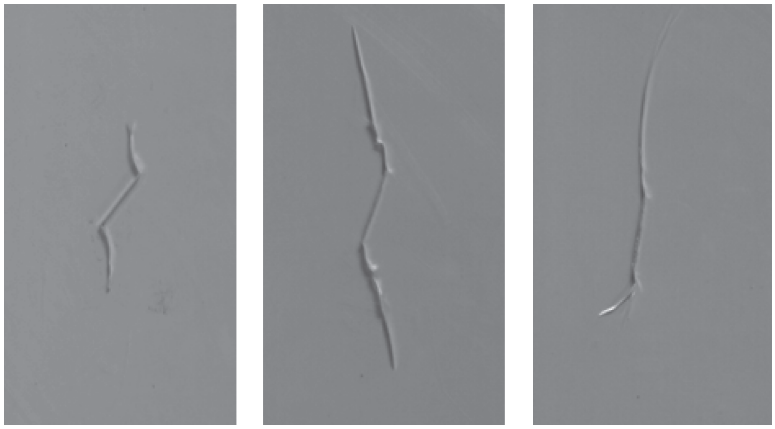

Fig. 3.15 (See color insert.) The breaking angle under different crack angles (acrylic material). (a) $\alpha = 45°$; (b) $\alpha = 70°$ (c) $\alpha = 80°$

When $\sigma_{\theta\theta\,\max}$ approaches to a critical point, the crack will unstably and quickly develop. Because $\sigma_{\theta\theta} \to \infty$ when $r \to 0$, so $\sigma_{\theta\theta\,\max}$ can't be used as a crack criterion this time. For mixed-model crack, an equivalent model-I crack can be used to as a crack criterion:

$$K_e = \frac{1}{2}\cos\frac{\theta_0}{2}[K_{\mathrm{I}}(1+\cos\theta_0) - 3K_{\mathrm{II}}\sin\theta_0]$$

and the failure criterion is $K_e = K_{\mathrm{I}C}$.

When crack is pure Model-II, by substituting $K_{\mathrm{I}} = 0$ and $\theta_0 = \arccos(1/3)$, $K_{\mathrm{II}} = K_{\mathrm{II}C}$, one can have:

$$\frac{K_{\mathrm{II}C}}{K_{\mathrm{I}C}} = \frac{\sqrt{3}}{2}$$

3.5.2 Strain Energy Density Theory

Suppose K_{I}, K_{II} and $K_{\mathrm{III}} \neq 0$ so the stress components around the crack tip are

$$\begin{aligned}
\sigma_x &= \frac{K_{\mathrm{I}}}{\sqrt{\pi r}}\cos\frac{\theta}{2}\left(1-\sin\frac{\theta}{2}\sin\frac{3\theta}{2}\right) - \frac{K_{\mathrm{II}}}{\sqrt{2\pi r}}\sin\frac{\theta}{2}\left(2+\cos\frac{\theta}{2}\cos\frac{3\theta}{2}\right)\\
\sigma_y &= \frac{K_{\mathrm{I}}}{\sqrt{\pi r}}\cos\frac{\theta}{2}\left(1+\sin\frac{\theta}{2}\sin\frac{3\theta}{2}\right) + \frac{K_{\mathrm{II}}}{\sqrt{2\pi r}}\sin\frac{\theta}{2}\cos\frac{\theta}{2}\cos\frac{3\theta}{2}\\
\tau_{xy} &= \frac{K_{\mathrm{I}}}{\sqrt{\pi r}}\cos\frac{\theta}{2}\sin\frac{\theta}{2}\cos\frac{3\theta}{2}\right) + \frac{K_{\mathrm{II}}}{\sqrt{2\pi r}}\cos\frac{\theta}{2}\left(1-\sin\frac{\theta}{2}\sin\frac{3\theta}{2}\right)
\end{aligned}$$

$$\tau_{xz} = \frac{K_{\mathrm{III}}}{\sqrt{\pi r}} \sin\frac{\theta}{2}, \tau_{yz} = \frac{K_{\mathrm{III}}}{\sqrt{2\pi r}} \cos\frac{\theta}{2}$$
$$\sigma_{zz} = \begin{cases} 0, plain, stress \\ 2\mu \left[\dfrac{K_{\mathrm{I}}}{\sqrt{2\pi r}} \cos\dfrac{\theta}{2} \dfrac{K_{\mathrm{II}}}{\sqrt{2\pi r}} \sin\dfrac{\theta}{2} \right], \quad plain, strain \end{cases}$$

The strain energy density is

$$\begin{aligned} w = \frac{1}{2E}[&\sigma_{11}^2 + \sigma_{22}^2 + \sigma_{33}^2 + 2(1+\mu)(\sigma_{12}^2 + \sigma_{13}^2 + \sigma_{23}^2) \\ &-2\mu(\sigma_1\sigma_{22} + \sigma_{22}\sigma_{33} + \sigma_{11}\sigma_{33})] \end{aligned} \tag{3.65}$$

then one can have:

$$w = \frac{1}{r}[a_{11}K_{\mathrm{I}}^2 + a_{22}K_{\mathrm{II}}^2 + a_{33}K_{\mathrm{III}}^2 + 2a_{12}K_{\mathrm{I}}K_{\mathrm{II}}] = S/r$$

where

$$a_{11} = \frac{1}{16\pi\mu}[(3 - 4\mu - \cos\theta)(1 + \cos\theta)]$$
$$a_{11} = \frac{1}{16\pi\mu}[(3 - 4\mu - \cos\theta)(1 + \cos\theta)]$$
$$a_{12} = \frac{1}{16\pi\mu}[(\cos\theta - 1 + 2\mu)2\sin\theta]$$
$$a_{22} = \frac{1}{16\pi\mu}[4(1-\mu)(1-\cos\theta) + (1+\cos\theta)(3\cos\theta - 1)]$$
$$a_{33} = \frac{1}{4\pi\mu}$$

According to the theory, the crack will develop when $S_{\min}$ is large than a certain value S_c and $S_{\min}$ satisfies the condition below:

$$\frac{\partial S}{\partial\theta} = 0, \ \frac{\partial^2 S}{\partial^2\theta} > 0 \tag{3.66}$$

For mode II, $K_{\mathrm{I}} = K_{\mathrm{III}} = 0$ and

$$S = \frac{K_{\mathrm{II}}^2}{16\pi\mu}[4(1-\mu)(1-\cos\theta) + (1+\cos\theta)(3\cos\theta - 1)]$$
$$\frac{\partial S}{\partial\theta} = \frac{K_{\mathrm{II}}^2}{16\pi\mu}[(1 - 2\mu - 3\cos\theta)\sin\theta]$$
$$\frac{\partial^2 S}{\partial^2\theta} = \frac{K_{\mathrm{II}}^2}{16\pi\mu}[(1-2\mu)\cos\theta - 3\sin 2\theta]$$

From equation (3.66), one can get the solution:

$$\begin{cases} \theta = 0 \\ \cos\theta = (1-2\mu)/3 \end{cases}$$

and the second θ satisfies $\frac{\partial^2 S}{\partial^2 \theta}$, so θ_0 is:

$$\theta = \arccos[(1-2\mu)/3] \tag{3.67}$$

and

$$S_{\min} = K_{\mathrm{II}}^2 \frac{2(1-\mu)-\mu^2}{12\pi\mu} \tag{3.68}$$

3.6 Crack Growth under Dynamic loading

The basic equations of plane elastic-dynamics are as below.

$$\begin{aligned} \frac{\partial \sigma_x}{\partial x} + \frac{\partial \tau_{xy}}{\partial y} &= \rho \ddot{u} \\ \frac{\partial \tau_{xy}}{\partial x} + \frac{\partial \tau_y}{\partial y} &= \rho \ddot{v} \end{aligned} \tag{3.69}$$

The strain-displacement relations are

$$\varepsilon_x = \frac{\partial u}{\partial x}, \quad \varepsilon_y = \frac{\partial \nu}{\partial y}, \quad \varepsilon_{xy} = \frac{1}{2}\left(\frac{\partial u}{\partial y} + \frac{\partial \nu}{\partial x}\right) \tag{3.70}$$

and constitutive relations are:

$$\begin{aligned} \sigma_x &= \lambda(\varepsilon_x + \varepsilon_y) + 2G\varepsilon_x \\ \sigma_y &= \lambda(\varepsilon_x + \varepsilon_y) + 2G\varepsilon_y \\ \tau_{xy} &= 2G\varepsilon_{xy} \end{aligned} \tag{3.71}$$

and λ is given by

$$\lambda = \begin{cases} \lambda^*, planes - strain \\ \dfrac{2\lambda^* G}{\lambda^* + 2G}, \quad plane - stress \end{cases}$$

Where

$$\lambda^* = \frac{E\mu}{(1+\mu)(1-2\mu)}, \quad G = \frac{E}{2(1+\mu)}.$$

To analyze crack growth under a dynamic loading, we first analyze the stress and displacement fields near a stationary crack tip. Because the displacements are finite, their derivatives with respect to time are also bounded for stationary cracks. At the same time, the stresses and their derivatives with respect to spatial coordinates are singular at the crack tip. The left side terms in the equations of motion equation (3.54) thus dominate the inertial terms on the

right side. Hence in the near-tip region, the forms of the equations of motion are simplified as follows:

$$\begin{aligned}\frac{\partial \sigma_x}{\partial x}+\frac{\partial \tau_{xy}}{\partial y}&=0\\ \frac{\partial \tau_{xy}}{\partial x}+\frac{\partial \sigma_y}{\partial y}&=0\end{aligned} \tag{3.72}$$

Because the material is still considered to be linear elastic, the stress and displacement fields near the crack tip will be the same as those in the quasi-static linear elastic fracture mechanics. Hence, the inertial effect does not change the singularity structure of stress and displacement fields near the tip of a stationary crack under dynamic loading. The crack tip stress and displacement fields are given by

$$\begin{aligned}\sigma_x &= \frac{K_{\mathrm{I}}(t)}{\sqrt{\pi r}}\cos\frac{\theta}{2}\left(1-\sin\frac{\theta}{2}\sin\frac{3\theta}{2}\right)-\frac{K_{\mathrm{II}}(t)}{\sqrt{2\pi r}}\sin\frac{\theta}{2}\left(2+\cos\frac{\theta}{2}\cos\frac{3\theta}{2}\right)\\ \sigma_y &= \frac{K_{\mathrm{I}}(t)}{\sqrt{\pi r}}\cos\frac{\theta}{2}\left(1+\sin\frac{\theta}{2}\sin\frac{3\theta}{2}\right)+\frac{K_{\mathrm{II}}(t)}{\sqrt{2\pi r}}\sin\frac{\theta}{2}\cos\frac{\theta}{2}\cos\frac{3\theta}{2}\\ \tau_{xy} &= \frac{K_{\mathrm{I}}(t)}{\sqrt{\pi r}}\cos\frac{\theta}{2}\sin\frac{\theta}{2}\cos\frac{3\theta}{2}\right)+\frac{K_{\mathrm{II}}(t)}{\sqrt{2\pi r}}\cos\frac{\theta}{2}\left(1-\sin\frac{\theta}{2}\sin\frac{3\theta}{2}\right)\end{aligned} \tag{3.73}$$

and

$$\begin{aligned}u &= \frac{K_{\mathrm{I}}(t)}{8\mu\pi}\sqrt{2\pi r}\left[(2\kappa-1)\cos\frac{\theta}{2}-\cos\frac{3\theta}{2}\right]\\ &\quad+\frac{K_{\mathrm{II}}(t)}{8\mu\pi}\sqrt{\pi r}\left[(2\kappa+3)\sin\frac{\theta}{2}+\sin\frac{3\theta}{2}\right]\\ v=u &= \frac{K_{\mathrm{I}}(t)}{8\mu\pi}\sqrt{2\pi r}\left[(2\kappa+1)\sin\frac{\theta}{2}-\sin\frac{3\theta}{2}\right]\\ &\quad+\frac{K_{\mathrm{II}}(t)}{8\mu\pi}\sqrt{\pi r}\left[(2\kappa-3)\cos\frac{\theta}{2}+\cos\frac{3\theta}{2}\right]\end{aligned} \tag{3.74}$$

where $K_{\mathrm{I}}(t)$ and $K_{\mathrm{II}}(t)$ are the dynamic stress intensity factors and (r,θ) are the polar coordinates at the crack tip with crack surfaces at $\theta=\pm\pi\cdot K_{\mathrm{I}}(t)$. and $K_{\mathrm{II}}(t)$ depend not only on the magnitude of the dynamic load and crack configuration, but also time t. In general, the peak values of the dynamic stress intensity factors for a given crack are higher than the corresponding SIF under the quasi-static loading of the same magnitude.

The monographs by Sih et al. (1972) and Freund (1990) provide the dynamic stress intensity factor solutions for various cracks under crack face impact loads and wave loads. Closed-form solutions of dynamic stress intensity factors are available for only a few problems of dynamically loaded stationary cracks. Maue (1954) considered a semi-infinite crack under a sudden crack face pressure σ at

time $t = 0$ and gave the dynamic stress intensity factor as follows:

$$K_{\mathrm{I}}(t) = \frac{2\sqrt{2}}{\pi}\frac{c_R}{c_1}\sigma_0\sqrt{\pi c t} \tag{3.75}$$

where c_R is the Rayleigh surface wave speed, which is the smallest real root of the following equation:

$$\left(2 - \frac{c_R^2}{c_2^2}\right)^2 - 4\left(1 - \frac{c_R^2}{c_1^2}\right)^{1/2}\left(1 - \frac{c_R^2}{c_2^2}\right)^{1/2} = 0 \tag{3.76}$$

Note that $c_R < c_2 < c_1$. Equation (3.75) shows that the dynamic stress intensity factor depends on both dilatational and Rayleigh surface wave speeds. Moreover, the dynamic stress intensity factor is zero at the beginning of loading and increases with time.

The crack tip stress field equation (3.73) shows that similar to the quasi-static cracks, the dynamic stress intensity factor determines the intensity of the singular stresses around the crack tip. the crack initiation thus can be predicted based on the SIF criterion, that is, the crack initiation occurs when the dynamic stress intensity factor reaches the dynamic fracture toughness of the material $K_{\mathrm{I}d}$.

$$K_{\mathrm{I}}(t) = K_{\mathrm{I}d} \tag{3.77}$$

This fracture criterion is applicable to brittle materials such as engineering ceramics and rocks, as well as metals when small-scale yielding conditions prevail.

3.6.1 Dynamic Crack Propagation in Rock

In a linear elastic material, a crack will propagate unstably once it has initiated. The crack propagation will lead to dynamic failure of the material unless it is arrested. Studies of the stress and displacement fields near a propagating crack tip usually use a moving coordinate system (x_1, y_1) centered at the crack tip, as shown in Figure 3.16, where (x, y) is a fixed coordinate system and $a(t)$ is a current crack propagation distance. The two systems are related by

$$x_1 = x - a(t), \quad y_1 = y \tag{3.78}$$

The material derivative in the moving coordinates becomes

$$d(\ )/dt = \partial(\ )/\partial t - V \cdot \partial(\ )/\partial x_1 \tag{3.79}$$

where $V = \dot{a} = da/dt$ is the crack propagation speed.

Using equations. (3.78) and (3.79), the wave equations (3.69) in the moving coordinates can be written as follows:

$$\begin{aligned}\frac{\partial^2\varphi}{\partial x_1^2}+\frac{\partial^2\varphi}{\partial y_1^2}&=\frac{1}{c_1^2}\left(\frac{\partial^2\varphi}{\partial t^2}-2V\frac{\partial^2\varphi}{\partial x_1\partial t}-\dot{V}\frac{\partial\varphi}{\partial x_1}+V^2\frac{\partial^2\varphi}{\partial x_1^2}\right)\\ \frac{\partial^2\psi}{\partial x_1^2}+\frac{\partial^2\psi}{\partial y_1^2}&=\frac{1}{c_2^2}\left(\frac{\partial^2\psi}{\partial t^2}-2V\frac{\partial^2\psi}{\partial x_1\partial t}-\dot{V}\frac{\partial\psi}{\partial x_1}+V^2\frac{\partial^2\psi}{\partial x_1^2}\right)\end{aligned} \tag{3.80}$$

These equations can be simplified as

$$\begin{aligned}\alpha^2\frac{\partial^2\varphi}{\partial x_1^2}+\frac{\partial^2\varphi}{\partial y_1^2}&=\frac{1}{c_1^2}\left(\frac{\partial\varphi}{\partial t^2}-2V\frac{\partial^2\varphi}{\partial x_1\partial t}-\dot{V}\frac{\partial\varphi}{\partial x_1}\right)\\ \beta^2\frac{\partial^2\psi}{\partial x_1^2}+\frac{\partial^2\psi}{\partial y_1^2}&=\frac{1}{c_2^2}\left(\frac{\partial^2\psi}{\partial t^2}-2V\frac{\partial^2\psi}{\partial x_1\partial t}-\dot{V}\frac{\partial\psi}{\partial x_1}\right)\end{aligned} \tag{3.81}$$

where α and β are given by

$$\alpha=\sqrt{1-(V/c_1)^2},\quad \beta=\sqrt{1-(V/c_2)^2} \tag{3.82}$$

Note that $\alpha>\beta$ when $c_1>c_2$. When the stresses are singular at the moving crack tip, the terms on the left part of equation (3.81) dominate because the terms on the right part have weaker singularities. In the crack tip, equation (3.81) can be written as

$$\begin{aligned}\alpha^2\frac{\partial^2\varphi}{\partial x_1^2}+\frac{\partial^2\varphi}{\partial y_1^2}&=0\\ \beta^2\frac{\partial^2\psi}{\partial x_1^2}+\frac{\partial^2\psi}{\partial y_1^2}&=0\end{aligned} \tag{3.83}$$

Now we introduce two polar coordinate systems, (r_1,θ) and (r_2,θ), at the moving crack tip as show in Figure 3.16.

$$\begin{aligned}x_1&=r_1\cos\theta_1,\quad y_1=\frac{r_1}{\alpha}\sin\theta_1\\ x_1&=r_2\cos\theta_2,\quad y_1=\frac{r_2}{\beta}\sin\theta_2\end{aligned} \tag{3.84}$$

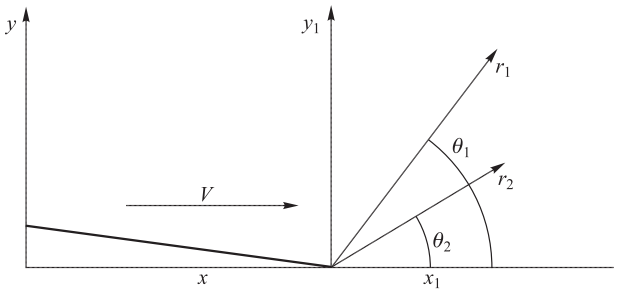

Fig. 3.16 Coordinate system on the moving crack tip.

thus,

$$\begin{aligned}\frac{\partial(\ )}{\partial x_1} &= \frac{\partial(\ )}{\partial r_1}\cos\theta_1 - \frac{\partial(\ )}{\partial \theta_1}\frac{\sin\theta_1}{\partial r_1} \\ \frac{\partial(\ )}{\partial y_1} &= \frac{\partial(\ )}{\partial r_1}\alpha\sin\theta_1 + \frac{\partial(\ )}{\partial \theta_1}\alpha\frac{\cos\theta_1}{r_1}\end{aligned} \tag{3.85}$$

in the (r_1, θ_1) system, and

$$\begin{aligned}\frac{\partial(\ )}{\partial x_2} &= \frac{\partial(\ )}{\partial r_2}\cos\theta_2 - \frac{\partial(\ )}{\partial \theta_2}\frac{\sin\theta_2}{\partial r_2} \\ \frac{\partial(\ )}{\partial y_2} &= \frac{\partial(\ )}{\partial r_2}\beta\sin\theta_2 + \frac{\partial(\ )}{\partial \theta_2}\beta\frac{\cos\theta_2}{r_2}\end{aligned} \tag{3.86}$$

in the (r_2, θ_2) system. Also we can have

$$\begin{aligned} r_1 &= \sqrt{x_1^2 + (\alpha y_1)^2}, \quad \theta_1 = \arctan\left(\frac{\alpha y_1}{x_1}\right) \\ r_2 &= \sqrt{x_1^2 + (\beta y_1)^2}, \quad \theta_2 = \arctan\left(\frac{\beta y_1}{x_1}\right)\end{aligned} \tag{3.87}$$

From these two equations, we can get:

$$\begin{aligned}&\frac{\partial r_1}{\partial x_1} = \frac{x_1}{r_1} = \cos\theta, \quad \frac{\partial r_1}{\partial y_1} = \frac{\alpha^2 y_1}{r_1} = \alpha\sin\theta_1 \\ &\frac{\partial \theta_1}{\partial x_1} = -\frac{\alpha y_1}{r_1^2} = -\frac{\sin\theta_1}{r_1}, \quad \frac{\partial \theta_1}{\partial y_1} = \frac{\alpha x_1}{r_1^2} = \alpha\frac{\cos\theta_1}{r_1} \\ &\frac{\partial \theta_2}{\partial x_1} = \frac{x_1}{r_2} = \cos\theta, \quad \frac{\partial r_2}{\partial y_1} = \frac{\beta^2 y_1}{r_1} = \beta\sin\theta_2 \\ &\frac{\partial \theta_2}{\partial x_1} = -\frac{\alpha y_1}{r_2^2} = -\frac{\sin\theta_2}{r_2}, \quad \frac{\partial \theta_2}{\partial y_1} = \frac{\beta x_1}{r_2^2} = \beta\frac{\cos\theta_2}{r_2}\end{aligned} \tag{3.88}$$

Since $\varphi = \varphi(r_1, \theta_1)$ and $\psi = \psi(r_2, \theta_2)$, equation (3.80) can be written as follows:

$$\begin{aligned}\frac{\partial^2 \varphi}{\partial r_1^2} + r_1\frac{\partial \varphi}{\partial r_1} + \frac{1}{r_1^2}\frac{\partial^2 \varphi}{\partial \theta_1^2} = 0 \\ \frac{\partial^2 \psi}{\partial r_2^2} + r_2\frac{\partial \varphi}{\partial r_2} + \frac{1}{r_2^2}\frac{\partial^2 \psi}{\partial \theta_2^2} = 0\end{aligned} \tag{3.89}$$

And the displacement potential functions are supposed to have the following form:

$$\begin{aligned}\varphi &= r_1^s\widetilde{\varphi}(\theta_1), \quad r_1 \to 0 \\ \psi &= r_2^s\widetilde{\psi}(\theta_2), \quad r_2 \to 0\end{aligned} \tag{3.90}$$

where s is the eigenvalue to be determined by the boundary conditions. Substituting equation (3.90) into equation (3.89), we have

$$\begin{aligned} \frac{d^2\widetilde{\varphi}}{d\theta_1^2} + s^2\widetilde{\varphi} = 0 \\ \frac{d^2\widetilde{\psi}}{d\theta_2^2} + s^2\widetilde{\psi} = 0 \end{aligned} \tag{3.91}$$

The general solutions of these equations are

$$\begin{aligned} \widetilde{\varphi} = C_1\cos(s\theta_1) + C_2\sin(s\theta_1) \\ \widetilde{\psi} = C_3\cos(s\theta_2) + C_4\sin(s\theta_2) \end{aligned} \tag{3.92}$$

In the following we consider Mode II crack propagation only. Mode II symmetry consideration gives $C_1 = C_4 = 0$. Hence equation (3.92) is simplified to

$$\begin{aligned} \widetilde{\varphi} = C_2\sin(s\theta_1) \\ \widetilde{\psi} = C_3\cos(s\theta_2) \end{aligned} \tag{3.93}$$

Substituting equation (3.90) into equation (3.86), and through the equations (3.84)–(3.88), we obtain the following asymptotic expressions for the displacement potential, displacement, and stressed at the moving crack tip:

$$\begin{aligned} \varphi &= A_2 r_1^2\sin(s\theta_1) \\ \psi &= A_3 r_2^s\cos(s\theta_2) \\ u &= sA_2 r_1^{s-1}\sin(s-1)\theta_1 - \beta sA_2 r_2^{s-1}\sin(s-1)\theta_2 \\ \nu &= \alpha sA_2 r_1^{s-1}\cos(s-1)\theta_1 - sA_3 r_2^{s-1}\cos(s-1)\theta_2 \end{aligned} \tag{3.94}$$

and

$$\begin{aligned} \sigma_{xx} &= (\lambda+2G)\frac{\partial u}{\partial x} + \lambda\frac{\partial \nu}{\partial y} \\ &= (\lambda+2G)[A_2 s(s-1)r_1^{s-2}\sin(s-2)\theta_1] - \\ &\quad \beta A_3 s(s-1)r_2^{s-2}\sin(s-2)\theta_2] + \\ &\quad \lambda[-\alpha^2 A_2 s(s-1)r_1^{s-2}\sin(s-2)\theta_1 + \\ &\quad \beta A_3 s(s-1)r_2^{r-2}\sin(s-2)\theta_2] \\ &= \rho c_2^2(2\alpha^2 + 1 - \beta^2)A_2 s(s-1)r_1^{r-2}\sin(s-2)\theta_1 - \\ &\quad 2\rho c_2^2\beta A_3 s(s-1)r_s^{s-2}\sin(s-2)\theta_2 \end{aligned}$$

$$\begin{aligned}\sigma_{yy} &= (\lambda+2G)\frac{\partial \nu}{\partial y}+\lambda\frac{\partial u}{\partial x} \\ &= (\lambda+2G)[-\alpha^2 A_2 s(s-1)r_1^{s-2}\sin(s-2)\theta_1 + \\ &\quad \beta A_3 s(s-1)r_2^{s-2}\sin(s-2)\theta_2] + \\ &\quad \lambda[A_2 s(s-1)r_1^{s-2}\sin(s-2)\theta_1 - \\ &\quad \beta A_3 s(s-1)r_2^{s-2}\sin(s-2)\theta_2] \\ &= \rho c_2^2(-1-\beta^2)A_2 s(s-1)r_1^{s-2}\sin(s-2)\theta_1 + \\ &\quad 2\rho c_2^2\beta A_3 s(s-1)r_2^{s-2}\sin(s-2)\theta_2 \\ \tau_{xy} &= G\left(\frac{\partial u}{\partial y}+\frac{\partial \nu}{\partial x}\right) \\ &= G[2\alpha A_2 s(s-1)r_1^{s-2}\cos(s-2)\theta_1 - \\ &\quad (1+\beta^2)A_3 s(s-1)r_2^{s-2}\cos(s-2)\theta_2]\end{aligned} \tag{3.95}$$

Because of the square root singularity, we can get

$$s = 3/2 \tag{3.96}$$

And for Model II, the displacements of crack surface should satisfy

$$\sigma_{yy} = 0, \quad \theta_1 = \theta_2 = \pi \tag{3.97}$$

Substituting equation (3.97) into equation (3.94), we can have the relation between A_2 and A_3 as follows

$$A_2 = \frac{2\beta}{1+\beta^2}A_3 \tag{3.98}$$

A_3 can be determined by the Model II dynamic stress intensity factor (SIF) $K_{\mathrm{II}}(t)$

$$A_3 = \frac{4}{3}\frac{K_{\mathrm{II}}(t)}{3G\sqrt{2\pi}}f, \quad f = \frac{1+\beta^2}{4\alpha\beta-(1+\beta^2)^2} \tag{3.99}$$

with $K_{\mathrm{II}}(t)$ is defined by

$$K_{\mathrm{II}}(t) = \lim_{r\to 0}\sqrt{2\pi r}\tau_{xy}(r_1, r_2, \theta_1, \theta_2)\Big|_{\theta_1=\theta_2=r_1=r_2=r=0}$$

The crack tip stress and displacement fields can be expressed

$$\begin{aligned}u &= \frac{2K_{\mathrm{II}}f}{G\sqrt{2\pi}}\left(\frac{2\beta}{1+\beta^2}\sqrt{r_1}\sin\frac{\theta_1}{2}-\beta\sqrt{r_2}\sin\frac{\theta_2}{2}\right) \\ \nu &= \frac{2K_{\mathrm{II}}f}{G\sqrt{2\pi}}\left(\frac{2\alpha\beta}{1+\beta^2}\sqrt{r_1}\cos\frac{\theta_1}{2}-\sqrt{r_2}\cos\frac{\theta_2}{2}\right)\end{aligned} \tag{3.100}$$

$$
\begin{aligned}
\sigma_{xx} &= \rho c_2^2(2\alpha^2+1-\beta^2)A_2 s(s-1)r_1^{s-2}\sin(s-2)\theta_1 \\
&\quad -2\rho c_2^2\beta A_3 s(s-1)r_2^{s-2}\sin(s-2)\theta_2 \\
&= \frac{K_{\mathrm{II}}f}{\sqrt{2\pi}}\left[-\frac{2\beta(2\alpha^2+1-\beta^2)}{1+\beta^2}\frac{1}{\sqrt{r_1}}\sin\frac{\theta_1}{2}+\frac{\beta}{\sqrt{r_2}}\sin\frac{\theta_2}{2}\right] \\
\sigma_{yy} &= \rho c_2^2(-1-\beta^2)A_2 s(s-1)r_1^{s-2}\sin(s-2)\theta_1 \\
&\quad +2\rho c_2^2\beta A_3 s(s-1)r_2^{s-2}\sin(s-2)\theta_2 \\
&= \frac{K_{\mathrm{II}}f}{\sqrt{2\pi}}\left[2\beta\frac{1}{\sqrt{r_1}}\sin\frac{\theta_1}{2}-\frac{\beta}{\sqrt{r_2}}\sin\frac{\theta_2}{2}\right] \\
\tau_{xy} &= G[2\alpha A_2 s(s-1)r_1^{s-2}\cos(s-2)\theta_1 \\
&\quad -(1+\beta^2)A_3 s(s-1)r_2^{s-2}\cos(s-2)\theta_2] \\
&= \frac{K_{\mathrm{II}}f}{\sqrt{2\pi}}\left[\frac{4\alpha\beta}{1+\beta^2}\frac{1}{\sqrt{r_1}}\cos\frac{\theta_1}{2}-(1+\beta^2)\frac{1}{\sqrt{r_2}}\cos\frac{\theta_2}{2}\right]
\end{aligned}
\tag{3.101}
$$

The crack tip velocity field can also be obtained by equation (3.80) ($\partial u/\partial t = 0$)

$$
\dot{u} = -\frac{VK_{\mathrm{II}}}{G\sqrt{2\pi}}\left(-\frac{\beta}{1+\beta^2}\frac{1}{\sqrt{r_1}}\sin\frac{\theta_1}{2}+\frac{\beta_1}{2}+\frac{\beta}{2\sqrt{r_2}}\sin\frac{\theta_2}{2}\right) \tag{3.102}
$$

3.7 Cohesive Model in Rock Fracture

Linear elastic fracture mechanics (LFEM) is valid only as long as nonlinear material deformation is confined to a small region around the crack tip. In many materials (such as iron, concrete, and rock), it is impossible to characterize the fracture behavior with LEFM.

Elastic-plastic fracture mechanics applies to materials that is related to time-independent, nonlinear behavior. In order to remove the singularity near the crack tip, Barenblatt (1962) gave a cohesive model, which considers the cohesive stress $g(x)$ near the crack tip, as shown in Figure 3.17.

Suppose K_{II} is the SIF which is related to the cohesive stress $g(x)$

$$
K'_{\mathrm{II}} = \frac{-2\sqrt{a}}{\sqrt{\pi}}\int_c^a \frac{g(x)dx}{\sqrt{a^2-x^2}}
$$

In order to remove the singularity near the crack tip, K'_{II} should be equal to K_{II},

$$
K_{\mathrm{II}} = -K'_{\mathrm{II}} = \frac{2\sqrt{a}}{\sqrt{\pi}}\int_c^a \frac{g(x)dx}{\sqrt{a^2-x^2}} \tag{3.103}
$$

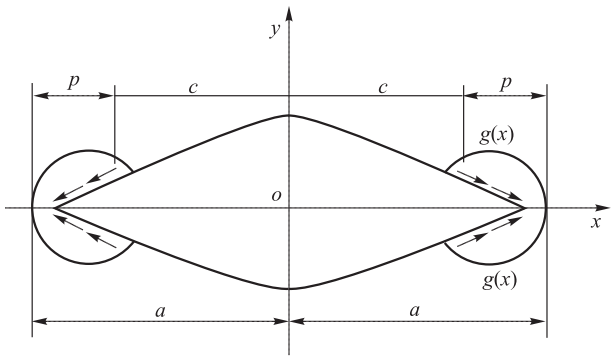

Fig. 3.17 Barenblatt cohesive model.

3.7.1 Stress change in slip-weakening model

The seismic fault failure can cause additional static stress around the crack tip. It is believed that the Coulomb failure stress change generated by earthquakes will have impact on the other remote earthquakes (Andrews, 1976; Aki and Richards, 1980; Chen and Knopoff, 1986; Harris, 1998, 2000; He et al., 2011). The Slip-weakening model (the extension of Barenblatt Cohesive Model) is used to examine the calculations of the Coulomb failure stress change.

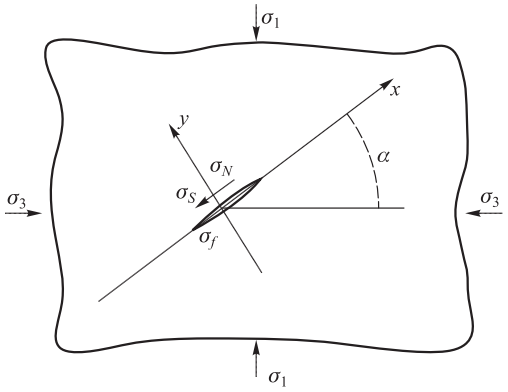

Fig. 3.18 Seismic fault under compression.

A seismic fault under compression is shown in Figure 3.18, where σ_s is the shear strength; σ_d is the sliding friction force; σ_f is the static friction force; $\Delta\sigma_e = \sigma_s - \sigma_d$ is the effective stress drop.

Suppose the shear stress at the fault surface increases to σ_s and then drops to σ_d, the effective stress drop $\Delta\tau_e = \sigma_s - \sigma_d$ will be determined in the earthquake wave data (*see* Fig. 3.19). The Coulomb stress change reflects the static stress

drop $\Delta\tau = \sigma_f - \sigma_d$, $0 < |x| < a$ so a coefficient can be written as (Andreev, 1995; He, 1995).

$$\gamma = \frac{\Delta\tau}{\Delta\tau_e} \tag{3.104}$$

Then

$$\Delta\tau = \gamma\Delta\tau_e \tag{3.105}$$

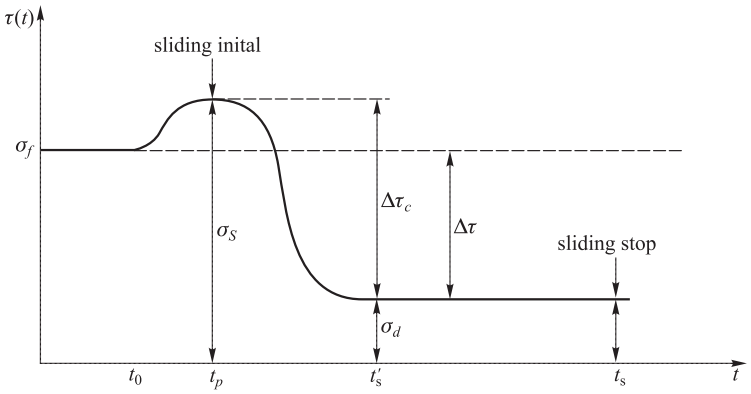

Fig. 3.19 Shear stress variation with time at a point on the fault surface (Yamashita 1976; Knopoff and Chen 2009).

For most of the time, the σ_d is not a constant, so $\Delta\tau = \sigma_f - \sigma_d(x)$, and the distribution in the fault surface is as below.

$$\sigma_d(x) = \begin{cases} \sigma_d, & |x| < c \\ \sigma(x), & c < |x| < a \end{cases}$$

Then the static stress drop $\Delta\tau = \sigma_f - \sigma_d(x)$ can be written as

$$\Delta\tau = \begin{cases} \sigma_f - \sigma_d, & |x| < c \\ \sigma_f - \sigma_d(x), & c < |x| < a \end{cases} \tag{3.106}$$

and the stress function of the additional stress field can be written as

$$Z_{\mathrm{II}} = \frac{2z}{\pi\sqrt{z^2 - a^2}} \int_0^a \frac{\sqrt{a^2 - \xi^2}}{z^2 - \xi^2} \Delta\tau(\xi) d\xi \tag{3.107}$$

$$Z_{\mathrm{II}} = \frac{2}{\pi} \int \frac{2z}{\pi\sqrt{z^2 - a^2}} \int_0^a \frac{\sqrt{a^2 - \xi^2}}{z^2 - \xi^2} \Delta\tau(\xi) d\xi \tag{3.108}$$

and the SIF on the both crack tips under the cohesive stress are the same because of the stress symmetry.

$$K_{\mathrm{II}}^+ = K_{\mathrm{II}}^- = \frac{2\sqrt{a}}{\sqrt{\pi}} \int_0^a \frac{\Delta\tau(\xi) d\xi}{\sqrt{a^2 - \xi^2}} \tag{3.109}$$

Substituting equation (3.108) into equation (3.25), the shear stress outside the fault surface can be shown:

$$\tau_{xy} = \frac{2x}{\pi\sqrt{x^2-a^2}} \int_0^a \frac{\sqrt{a^2-\xi^2}\Delta\tau(\xi)d\xi}{x^2-\xi^2}, \quad x| > a,\ y = 0 \tag{3.110}$$

By utilizing equation

$$\frac{\sqrt{a^2-\xi^2}}{z^2-\xi^2} = \frac{1}{\sqrt{a^2-\xi^2}} - \frac{x^2-a^2}{(x^2-\xi^2)\sqrt{a^2-\xi^2}},$$

the shear stress can be expressed as below.

$$\tau^c_{xy} = \frac{2x}{\pi\sqrt{x^2-a^2}} \int_0^a \frac{\Delta\tau(\xi)d\xi}{\sqrt{a^2-\xi^2}} - \frac{2x\sqrt{x^2-a^2}}{\pi} \int_0^a \frac{\Delta\tau(\xi)d\xi}{(x^2-\xi^2)\sqrt{a^2-\xi^2}}, \quad |x| > a,\ y = 0 \tag{3.111}$$

The first part in equation (3.111) should be zero because there is no singularity after the cohesive stress being introduced, so the shear stress τ^c_{xy} will be:

$$\tau^c_{xy} = \frac{2x\sqrt{x^2-a^2}}{\pi} \int_0^a \frac{\Delta\tau(\xi)d\xi}{(x^2-\xi^2)\sqrt{a^2-\xi^2}}, \quad |x| > a,\ y = 0 \tag{3.112}$$

For a real seismic fault, the crack surface is covered by all kinds of uneven cleavages, which makes $\Delta\tau(x)$ nonlinear and more complicated. From equation (3.112), one can find that the different distribution of $\Delta\tau(x)$ has no impact on the stress field τ^c_{xy}. It is the final result of the calculus that has the final impact on τ^c_{xy}.

For the linear distribution of the shear stress $\sigma_d(x)$ along the crack surface (see Fig. 3.20),

$$\sigma_d(x) = \begin{cases} \gamma_d, & |x| < c \\ \sigma_s - (\sigma_s - \sigma_d)\dfrac{a-x}{a-c}, & c < |x| < a \end{cases} \tag{3.113}$$

The corresponding static stress drop can be written as

$$\Delta\tau = \begin{cases} \gamma(\sigma_s - \sigma_d), & |x| < c \\ \left(\gamma - \dfrac{x-c}{a-c}\right)(\sigma_s - \sigma_d), & c < |x| < a \end{cases} \tag{3.114}$$

Substituting equation (3.114) into equation (3.107) and (3.108), one can have the shear stress ($|x| > a, y = 0 |x| > a, y = 0$)

$$\tau^c_{xy} = (\sigma_s - \sigma_d)\left(-\gamma + \frac{2}{\pi(a-c)}\left[x\arctan\sqrt{\frac{a^2-c^2}{x^2-a^2}} - c\arctan\frac{x}{c}\sqrt{\frac{a^2-c^2}{x^2-a^2}}\right]\right) \tag{3.115}$$

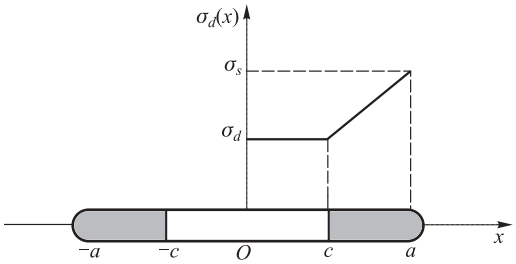

Fig. 3.20 Linear distribution of $\sigma_d(x)$ along a fault surface.

At the crack surface ($|x| < a, y = 0$), the shear stress is

$$\tau_{xy}^{c} = -\Delta\tau = -(\sigma_s - \sigma_d)\left(\gamma - \frac{x-c}{a-c}\right), \quad |x| < a,\ y = 0 \tag{3.116}$$

Substituting equation (3.74) into equation (3.71), one have

$$\widetilde{Z}_{\mathrm{II}} = \frac{2(\sigma_s - \sigma_d)}{\pi(a-c)}\left[-\frac{\pi c^2}{4} - \frac{\pi\gamma(a-c)z}{2} + A\sqrt{z^2-a^2} + \frac{z^2+c^2}{4i}\ln\frac{\sqrt{z^2-a^2}+i\sqrt{a^2-c^2}}{\sqrt{z^2-a^2}-i\sqrt{a^2-c^2}} - \frac{cz}{2i}\ln\frac{c\sqrt{z^2-a^2}+iz\sqrt{a^2-c^2}}{c\sqrt{z^2-a^2}-iz\sqrt{a^2-c^2}}\right] \tag{3.117}$$

At the crack surface

$$y = 0, \quad \theta_1 = \pi, \quad \theta_2 = 0, \quad r_1 = a - x, \quad r_2 = a + x, \quad \sqrt{z^2-a^2} = i\sqrt{a^2-x^2},$$

the displacement (plain strain) on the crack upper surface is

$$u^{c+} = \frac{2(1-\mu)}{\pi G}\frac{(\sigma_s - \sigma_d)}{(a-c)}\left[A\sqrt{a^2-x^2} + \frac{x^2+c^2}{4}\ln\frac{\sqrt{a^2-x^2}+\sqrt{a^2-c^2}}{\sqrt{a^2-x^2}-\sqrt{a^2-c^2}} - \frac{cx}{2}\ln\left|\frac{x\sqrt{a^2-c^2}+c\sqrt{a^2-x^2}}{x\sqrt{a^2-c^2}-c\sqrt{a^2-x^2}}\right|\right], \quad A = \frac{\sqrt{a^2-c^2}}{2}$$

$$\nu^{c+} = \frac{(1-2\mu)}{\pi G}\frac{(\sigma_s - \sigma_d)}{(a-c)}\left[\frac{c^2}{2} + \gamma(a-c)x\right], \tag{3.118}$$

and the displacement on the crack bottom surface

$$\begin{aligned} u^{c-} &= -u^{c+} \\ \nu^{c-} &= \nu^{c+}, \end{aligned} \tag{3.119}$$

The displacement change between the upper and bottom surfaces are

$$\begin{aligned} \Delta u^{c-} &= 2u^{c+} \\ \Delta\nu &= 0 \end{aligned} \tag{3.120}$$

3.7.2 Relationship between Energy Release Rate G and the Parameter in Slip-weakening Model

The stress distribution near the crack tip is shown in Fig. 3.21, the stress drops from σ_s to σ_d (slip-weakening zone from c to a), and the displacement reaches to its maximum δ^*. If we apply J-integral along the crack tip from bottom surface to upper surface and consider the disappearance of singularity at the crack tip, we have the result from Section 3.4.2

$$0 = J_Q + \int_Q^0 \left(\sigma \frac{\partial \delta}{\partial x_1} dx_1\right) \tag{3.121}$$

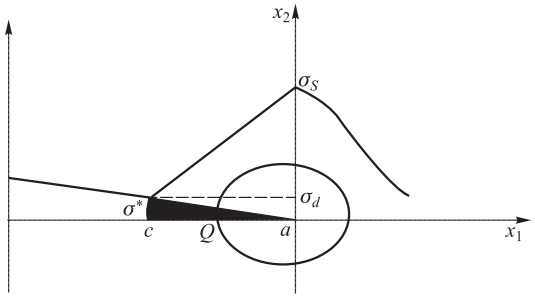

Fig. 3.21 The stress distribution near the crack.

According to the equation (3.73), the second part of the equation above can be written as

$$\int_Q^0 \left(\sigma(\delta) \frac{\partial \delta}{\partial x_1}\right) = -\int_0^{\delta^*} [\sigma(\delta) - \sigma^d] \frac{\partial \delta}{\partial x_1} dx_1 - \sigma^d \delta_Q \tag{3.122}$$

where Q is the beginning and end point of the closure.

From equation (3.122), the equation (3.121) can be converted to

$$J_Q - \sigma^d \delta_Q = \int_0^{\delta^*} [\sigma(\delta) - \sigma^d] \frac{\partial \delta}{\partial x_1} dx_1 \tag{3.123}$$

The left part is independent of and can be considered as the driving force. The right part can be reckoned as the resisting force, so equation (3.108) can be thought of being a criterion of crack growth. From equation (3.58), the equation (3.123) can be converted to

$$G = J_Q - \sigma^d \delta_Q = [\sigma^s - \sigma^d] \overline{\delta}$$

where δ is the average displacement of the slip-weakening zone (from c to a), which means G can be got from multiplier of the stress drop and the average

displacement $\overline{\delta}$.

$$J_\theta - \sigma^d \delta_Q = \int_0^{\delta^*} [\sigma(\delta) - \sigma^d] \frac{\partial \delta}{\partial x_1} dx_1$$

3.8 Numeric Method for Fracture Mechanics

The numeric method, especially for finite element method (FEM), is an effective tool to solve some complex problems, such as objects with complicated surfaces, or fluid-solid coupling problems. Compared to other numeric methods, FEM has its own advantages so that it is wildly used in fracture mechanics. However, the conventional finite element method considers the crack surface as the border of elements and treats the crack tip as a node of an element. These treatments increase the complex of computation. In order to solve this problem, some new thoughts are introduced to deal with the crack surface problems. Among them, the the singularity element and the extended finite element method (XFEM) are reckoned as the commonly used strategies.

3.8.1 Singularity Element Method

A significant advancement in FEM was the simultaneous and independent "quarter-point" elements developed by Henshell and Shawn (1975), Barsoum (1976), Hibbitt (1977), and Hoenig (1982). In their method, the proper crack-tip displacement, stress and strain fields are modeled by the standard quadratic order iso-parametric finite elements if one moves the element's mid-side node to the position by one quarter of the way from the crack tip to the far end of the element. This procedure introduces a singularity into the mapping between the element's parametric coordinate space and the Cartesian space. Henshell and Shaw (1975) described a quadrilateral quarter-point element, illustrated in Figure 3.22a. Barsoum (1977) proposed collapsing one edge of the element at the crack tip. This is shown in Figure 3.22b, where the crack-tip nodes (1, 4 and 8) are constrained to move together. The discovery of the quarter-point elements was a significant milestone in the development of FEM. With these elements standards, FEM can be used to model the crack tip fields accurately with only minimal modification.

The effect of moving the side node of a quadratic element to the quarter-point position can be best illustrated with a one-dimensional element. A one-dimensional quadratic order element is illustrated in Figure 3.23. The displace-

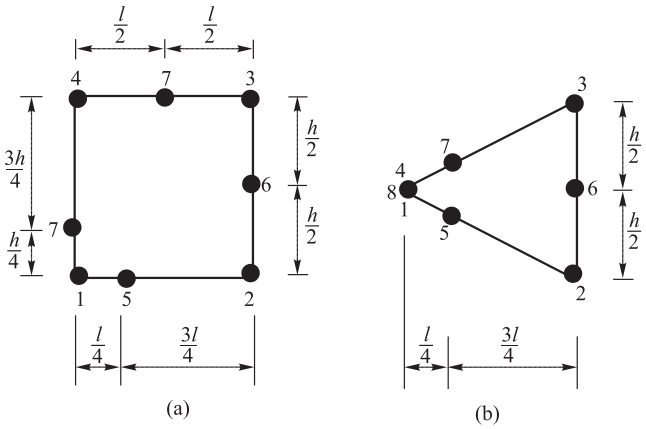

Fig. 3.22 (a) Quadrilateral and (b) collapsed quadrilateral quarter-point elements.

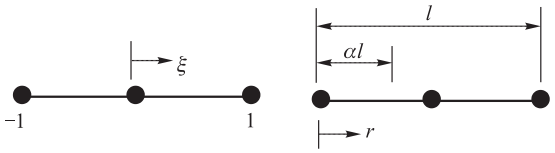

Fig. 3.23 (a) the parametric space and (b) the Cartesian space of the element.

ment u at any point within the element is determined by interpolating the nodal displacements, u_i using the standard lagrange second order shape functions,

$$u = \sum_{i=1}^{3} N_i u_i = \frac{1}{2}\xi(\xi-1)u_1 + (1-\xi^2)u_2 + \frac{1}{2}\xi(\xi+1)u_3$$

or

$$u = u_2 + \frac{1}{2}(u_3 - u_1)\xi + \left[\frac{1}{2}(u_3 + u_1) - u_2\right]\xi^2 \tag{3.124}$$

Using an iso-parametric formulation, the same shape functions are used to interpolate the geometry of the element:

$$r = \sum_{i=1}^{3} N_i r_i = \alpha l + \frac{1}{2}I\xi + \left(\frac{1}{2}I - \alpha I\right)\xi^2 \tag{3.125}$$

First, consider the case where the center node is located at the mid-point of the element. That is $\alpha = 1/2$ and $r = I(1+\xi)/2$. Substituting this expression for ξ into equation (3.124) yields the expected quadratic expression in r for the displacements

$$u = u_1 + (4u_2 - u_3 - 3u_1)\frac{r}{l} + 2(u_3 + u_1 - 2u_2)\frac{r^2}{l^2} \tag{3.126}$$

Differentiating this expression yields the expected linear expression in r for the strains in the element

$$\varepsilon = \frac{du}{dr} = (4u_2 - u_3 - 3u_1)\frac{1}{l} + 4(u_3 + u_1 - 2u_2)\frac{r}{l^2}.$$

Then consider the case where the middle node is moved to the quarter-point position. For this case, $\alpha = 1/4$ and $\xi = \frac{2\sqrt{lr}}{l} - 1$. Substituting this expression for ξ into equation (3.109) and differentiating yields the following expressions for the displacements and strains in the element

$$\begin{aligned} u &= u_1 + 2(u_3 + u_1 - 2u_2)\frac{r}{l} + (u_3 - 3u_1 + 4u_2)\frac{\sqrt{rl}}{l} \\ \varepsilon &= \frac{du}{dr} = 2(u_3 + u_1 - 2u_2)\frac{1}{r} + \left(2u_2 - \frac{3}{2}u_1 - \frac{1}{2}u_3\right)\frac{1}{lr} \end{aligned} \tag{3.127}$$

One can see that the three terms in the displacement expression model a constant value, a linear variation in , and the square root variation in . This corresponds to the leading terms in the LFEM expressions for the near crack-tip displacement. The expression for the strains contains a constant term and a singular term that varies as , the form of lead term in the LEFM stress and strain expansions.

For two dimension (see Fig. 3.24), the displacements along the crack face for the quarter-point element interpolation are

$$\begin{aligned} \nu_{\text{upper}} &= \nu_a + (2\nu_a + 2\nu_c - 4\nu_b)\frac{r}{l} + (4\nu_b - \nu_c - 3\nu_a)\frac{\sqrt{rl}}{l} \\ \nu_{\text{ower}} &= \nu_a + (2\nu_a + 2\nu_e - 4\nu_d)\frac{r}{l} + (4\nu_d - \nu_e - 3\nu_a)\frac{\sqrt{rl}}{l} \end{aligned}$$

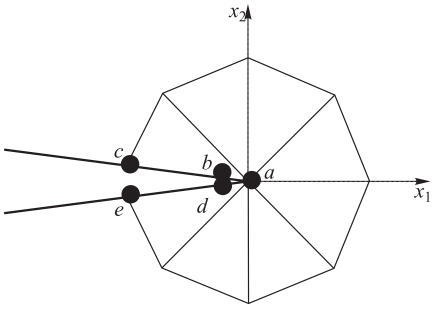

Fig. 3.24 Two dimensional singularity element at the crack tip.

The FEM crack opening displacement (COD) is

$$\nu_{\text{upper}} - \nu_{\text{lower}} = [4(\nu_b - \nu_d) + 2(\nu_c - \nu_e)]\frac{r}{l} + [4(\nu_b - \nu_d) - \nu_c + \nu_e]\frac{\sqrt{rl}}{l}$$

The square root term of the COD can then be substituted into the analytical crack-tip displacement field to yield

$$\begin{aligned} K_{\mathrm{I}} &= \frac{G\sqrt{2\pi}}{(2-2\mu)\sqrt{r}}[4(\nu_b-\nu_d)+\nu_e-\nu_c], \\ K_{\mathrm{II}} &= \frac{G\sqrt{2\pi}}{(2-2\mu)\sqrt{r}}[4(\nu_b-\nu_d)+u_e-u_c], \end{aligned} \tag{3.128}$$

3.8.2 Extended Finite Element Method

The extended finite element method (XFEM) retains all advantages of the common finite element method (CFEM), and overcomes difficulties in meshing and re-meshing within the crack tip region that contains the stress concentration. XFEM uses the partition of unity framework (Moes et al., 1999, 2003; Babuska and Melenk, 1997) to model strong and weak discontinuities independent of the finite element mesh (see Fig. 3.25). This allows discontinuous functions to be implemented into a traditional finite element framework through the use of enrichment functions and additional degrees of freedom.

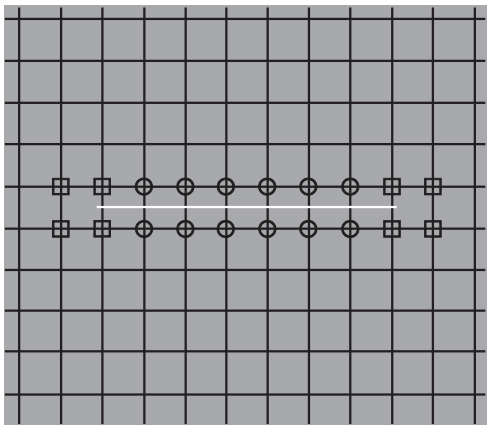

Fig. 3.25 Enriched nodes for crack.

Cracks are modeled using a combination of two enrichment functions. One for the complicated behavior at the crack tip and another is a Heaviside step function to represent the discontinuity across the body of the crack. The Heaviside function takes a value of 1 above the crack and -1 below the crack, thus putting a displacement discontinuity across the body of the crack in elements whose support is cut by the crack. For the crack tip the enrichment functions originally introduced by Fleming et al. (1997) for use in the element free Galerkin

method. They were later adopted by Belytschko et al. (2001) for use in XFEM. These four functions span the crack tip displacement field. Also note that the first function is discontinuous across the crack within the element containing the crack tip. For information on modeling bi-material or branching cracks please refer to the papers by Sukumar et al. (2001) and Daux (2000).

The XFEM displacement approximation for a domain with a crack takes the following form.

$$u^h(x) = \sum_{\mathrm{I}\in N} N_{\mathrm{I}}(x) \left[u_{\mathrm{I}} + H(x)a_{\mathrm{I}} + \sum_{J=1}^{4} F_J(x) b_{\mathrm{I}}^J \right] \tag{3.129}$$

where u_{I} is Nodal DOF; N_{I} is Shape Function; a_{I} is Nodal enriched DOF; b_{I}^J is Nodal DOF at the crack tip enrichment;

$$H(x) = \begin{cases} 1, & if(x - x^*) \cdot n \geqslant 0 \\ -1, & otherwise \end{cases} \text{ is Heaviside function}$$

and $F_J(x) = \left[\sqrt{r}\sin\frac{\theta}{2}, \sqrt{r}\cos\frac{\theta}{2}, \sqrt{r}\sin\theta\sin\frac{\theta}{2}, \sqrt{r}\sin\theta\cos\frac{\theta}{2}\right]$ is the crack tip asymptotic functions.

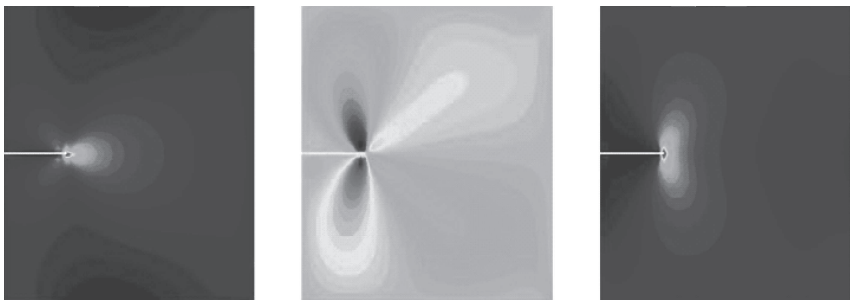

(a) (b) (c)

Fig. 3.26 (See color insert.) Edge crack under bi-axial tension. (a) σ_x; (b) σ_{xy}; (c) σ_y.

Predicting where a crack will initiate is a challenging area of computational mechanics. The most common approach is to place a crack at the location of maximum stress (Edke and Chang, 2010). However, it is well known that the stress fields from finite element simulations converge at a rate which is much slower than displacements. Therefore, it may be difficult, if not impossible, to identify the exact location of maximum stress. It is possible for an optimization problem to be formulated to identify the initial crack location. While in general this optimization problem may be too expensive to consider with regards to a finite element simulation with a large number of degrees of freedom, the use of the proposed reanalysis algorithm (Paris, 2010) makes the solution of the optimization problem possible.

3.9 Discussion

In this chapter, a crack model is established by using complex functions, and an analytical solution of the crack tip stress intensity factors for three cracks under compression has been presented. Coulomb-Mohr failure criterion, energy release and J-integral, as well as the numeric method have been analyzed. Generally, this chapter has presented some novel methods and techniques for the study of fault stability and earthquake. But the rock environment is so complex that many other factors need to be involved.

First, the properties of rocks will change dramatically when the depth increases because the temperature increases with it. The mechanism of the rock will be similar to that of the liquid, and the strength of it decrease sharply, and thus the strain and stress will change with the time, which is named as a creep. Compared to the linear or plastic theory, creep is more complicated and there is no universal theory until now because of its non-linear character.

Second, chemical effect of rock coupled with water is another important factor. The character of rock is reshaped when under water, so it is the mechanic property. A better understanding of it depend on the research of geochemistry.

Acknowledgments

On the completion of this chapter, we should like to express our deepest gratitude to all those whose kindness and advice have made this work possible.

References

Aki K., Richards P.G., 1980. Quantitative Seismology, Theory and Method. San Francisco H Freeman Company, 867.

Andreev G.E., 1995. Brittle Failure of Rock Materials. Balkema, Rotterdam.

Anderson T.L., 1995. Fracture Mechanics: Fundamentals and Applications. CRC Press.

Andrews D.J., 1976. Rupture velocity of plane-strain shear cracks. J Geophysics Res, 81(B32): 5679–5687.

Ashby M.F., Hallam S. D., 1986. The failure of brittle solids containing small cracks under compressive stress states. Acta Metallica, 34: 497–510.

Babuska I., Melenk J., 1997. The partition of unity method, International Journal for Numerical Methods in Engineering, 40: 727–758.

Ballarini R., Plesha E.M., 1987. The effects of crack surface friction and roughness on crack tip stress fields, Int. J. Fract, 34: 195–207.

Barenblatt G.I., 1962. The mathematical theory of equilibrium cracks in brittle fracture. Advances in Applied Mechanics, 7: 55–129.

Barsoum R.S., 1976. On the use of isoparametric finite elements in linear fracture mechanics. Int. J. Num. Meth. Engng, 10: 25–37.

Barsoum R.S., 1977. Triangular quarter-point elements as elastic and perfectly-plastic crack tip elements. Int. J. Num. Meth. Engng., 11: 85–98. Basista M., Gross D., 2000. A note on crack interactions under compression, Int. J. Fract, 102: 67–72.

Baud P., Reuschle T., Charleg P., 1996. An improved wing crack model for the deformation and failure of rock in compression. International Journal of Rock Mechanics and Mineral Science Geomechanics, 33: 539–542.

Belytschko T., Moes N., Usui S., Parimi C., 2001. Arbitrary discontinuities in finite elements. International Journal for Numerical Methods in Engineering, 50: 993–1013.

Buckley C.P., 2005. Material Failure, Lecture Notes. University of Oxford.

Camacho G.T., Ortiz, M., 1997. Computational modelling of impact damage in brittle materials. International Journal of Solids and Structures, 33 (20-22): 289–298.

Chen Y T, Knopoff L. 1986. Static shear crack with a zone of slip weakening. Geophysics J. R. astr. Soc., 87(3): 1005–1024.

Chen Y.Z., Hasebe N., Lee K.Y., 2003. Multiple Crack Problems in Elasticity. WIT Press, Southampton.

Cherepanov G. P., 1967. The propagation of cracks in a continuous medium. Journal of Applied Mathematics and Mechanics, 31(3): 503–512.

Daux C., Moes N., Dolbow J., Sukumar N., Belytschko T., 2000. Arbitrary branched and intersecting cracks with the extended finite element method. International Journal for Numerical Methods in Engineering, 48: 1741–1760.

Dugdale D.S., 1960, Yielding of steel sheets containing slits. Journal of the Mechanics and Physics of Solids, 8 (2): 100–104.

Eberhardt A. W., Kim B.S., 1998. Crack face friction effects on mode II stress intensities for a surface-cracked coating in two dimensional rolling contact. Tribol. Trans., 41: 35–42.

Edke M.S., Chang K.H., Shape sensitivity analysis for 2-D mixed mode fractures using extended FEM (XFEM) and level set method (LSM). International Journal of Mechanics Based Design of Structures and Machines, EISSN: 1539–7742.

England A.H., 1971. Complex Variable Methods in Elasticity. Wiley-Interscience, New York.

Erdogan F., 1962. On the stress distribution in plates with collinear cuts under arbitrary loads, in Proceedings of the 4th U.S. National Congress of Applied Mechanics, Vol. 1, 547–553.

American Society of Mechanical Engineers, New York.

Erdogan E., 2000. Fracture Mechanics. International Journal of Solids and Structures, 37: 171–183.

Fan T. Y., 2003, Fundamental of Fracture Theory, 56–57. Science Press, Beijing.

Fleming M., Chu A., Moran B., Belytschko T., 1997. Enriched element-free Galerkin

methods for crack tip fields. International Journal for Numerical Methods in Engineering, 40: 1483–1504.

Freund L.B., 1990. Dynamic fracture mechanics. Cambridge University Press, Cambridge, UK.

Germanovich L.N., Salganik R.L., Dyskin A.V., Lee K.K., 1994. Mechanisms of brittle fracture of rock with pre-existing cracks in compression. PHGEOPH, 143: 117–147.

Gong S.X., 1994. Micro crack interaction with a finite main crack: an exact formulation. International Journal of Fractures, 66: 51–66.

Griffith A.A. 1921. The phenomena of rupture and flow in solids. Philosophical Transactions of the Royal Society of London, A 221: 163–198.

Harris R.A., 1998. Introduction to special section: stress triggers, stress shadows, and seismic hazard. J. Geophys. Res., 103(B10): 24347–24358.

Harris R A., 2000. Earthquake stress triggers, stress shadows, and seismic hazard. Current Science, 79(9): 1215–1225.

He C.R., 1995. Slip weakening constitutive relation and the structure in the vicinity of a shear crack tip. Pure Apply Geophysics, 145(3–4): 747–757.

He T M, Chen Y T, Zhang H K., 2011. Coulomb failure stress change in slip weakening model and remote triggering of earthquakes. Acta Sersmiologica Sinica, 32(2): 165–186.

Henshell R.D., Shaw K.G., 1975. Crack tip finite elements are unnecessary. Int. J. Num. Meth. Engng., 9: 495–507.

Hibbitt H.D., 1977. Some properties of singular isoparametric elements. Int. J. Num. Meth. Engng., 11: 180–184.

Hoenig, 1982. Near-Tip behavior of a crack in a plane anisotropic elastic body. Engng. Fracture Mech., 16: 393–403.

Hutchinson J. W., 1968. Singular behavior at the end of a tensile crack in a hardening material, Journal of the Mechanics and Physics of Solids 16(1): 13–31.

Irwin G., 1957. Analysis of stresses and strains near the end of a crack traversing a plate. Journal of Applied Mechanics, 24: 361–364.

Jin W.C., Zhu Z.M., Gao M. Z., 2013. A general method to determine the stress intensity factor of multiple collinear cracks. Math.Mech. Solids, DOI: 10.1177/1081286512439556.

Kachanov M., 1987. Elastic solids with many cracks: A simple method of analysis. Int. J. Solids Struct. 23(1): 23–43.

Lauterbach B., Gross D., 1998. Crack growth in brittle solids under compression, Mech. Mater. 29: 81–92.

Lee, R. F., Donovan J. A., 1987. J-integral and crack opening displacement as crack initiation criteria in natural rubber in pure shear and tensile specimens. Rubber Chemistry and Technology, 60(4): 674–688.

Li C., Nordlund E., 1993. Deformation of brittle rocks under compression with particular reference to microcracks. Mechanics of Materials, 15: 223–239.

Li Y.P., Tham L.G., Wang Y.H., Tsui Y., 2003. A modified Kachanov method for analysis of solids with multiple cracks, Eng.Fract. Mech. 70: 1115–1129.

Maue A.W., 1954. Die entspannungswelle bei plotzlichem Einschnitt eines gespannten elastischen Korpers. Zeitschrift fur angewandte Mathematik und Mechanik, 34: 1–12.

Meyers, Chawla, 1999. Mechanical Behavior of Materials, 445–448.

Millwate H.R., 2010. A simple and accurate method for computing stress intensity factors of collinear interacting cracks. Aerospace Sci. Technol. 14: 542–550.

Moes N., Cloirec M., Cartraud P., Remacle J.F., 2003. A computational approach to handle complex microstructure geometries. Computer Methods in Applied Mechanics and Engineering, 192: 3163–3177.

Moes N., Dolbow J., Belytschko T., 1999. A finite element method for crack growth without remeshing. International Journal for Numerical Methods in Engineering, 46: 131–150.

Muskelishvili N.I., 1953. Some Basic Problems of Mathematical Theory of Elasticity., Noordhoff, Amsterdam.

Nemat-Nasser S., Horii H., 1982. Compression-induced nonplanar crack extension with application to splitting, exfoliation, and rock bust. Journal of Geophysical Research, 87(B8): 680–6821.

Newman J.C., 1971. An improved method of collocation for the stress analysis of cracked plate with various shaped boundaries. NASA TN D-6376.

Olver F.W., Lozier D.W., Boisvert R.F., Clark C.W., 2010. NIST Handbook of Mathematical Functions. 485–522, Cambridge University Press, Cambridge.

Orowan E., 1948. Fracture and strength of solids. Reports on Progress in Physics XII, 185rious Pais M., Kim N.H., Davis T., 2010. Reanalysis of the extended finite element method for crack initiation and propagation.51st AIAA/ASME/ASCE/AHS/ASC Structures, Structural Dynamics, and Materials Conference, Orlando, Florida.

Ramberg, Walter; Osgood, William R., 1943, Description of stress-strain curves by three parameters. US National Advisory Committee for Aeronautics, 902.

Rice R., 1968. A Path Independent Integral and the Approximate Analysis of Strain Concentration by Notches and Cracks. Journal of Applied Mechanics, 35: 379–386.

Rice J.R., 1968. Mathematical analysis in the mechanics of fracture, in: H. Liebowitz (Ed.), Fracture, Vol. 2: 191-311, Academic Press, New York.

Rice J.R., Lapusta N., Ranjith K., 2001. Rate and state dependent friction and the stability of sliding between elastically deformable solids. Journal of Mechanics and Physics of Solids, 49: 1865–1898.

Sih G.C., Embley G.T., Ravera R.S., 1972. Impact response of a finite crack in plane extension, Int. J. Sol. Struct. 8: 977–993.

Steif P.S., 1984. Crack extension under compressive loading. Engineering and Fracture Mechanics, 20: 463–473.

Sukumar N., Chopp D.L., Moes N., Belytschko T., 2001. Modeling holes and inclusions by level sets in the extended finite-element method. Computer Methods in Applied Mechanics and Engineering, 190: 6183–6200.

Van Vliet, Krystyn J., 2006. 3.032 Mechanical Behavior of Materials.

Wang R.D., 1997. The stress intensity factors of a rectangular plate with collinear cracks under uniaxial tension. Engineering and Fracture Mechanics, 56: 347–356.

Willis J.R., 1967. A comparison of the fracture criteria of Griffith and Barenblatt. Journal of the Mechanics and Physics of Solids 15 (3): 151–162.

Yoda M., 1980. The J-integral fracture toughness for Mode II, Int. J. of Fracture, 16(4): R175-R178.

Zhu Z., Wang L., Mohanty B., Huang C., 2006. Stress intensity factor for a cracked specimen under compression. Engineering and Fracture Mechanics, 73: 482–489.

Zhu Z., 1999. New biaxial failure criterion for brittle materials in compression. Journal of Engineering Mechanics, 125: 1251–1258.

Zhu Z., Ji S., Xie H.., 1996 An improved method of collocation for the problem of crack surface subjected to uniform load, Engineering and Fracture Mechanics, 54: 731–741.

Zhu Z., Xie H., Ji S., 1997. The mixed boundary problems for a mixed mode crack in a finite plate. Engineering and Fracture Mechanics, 56: 647–655.

Authors Information

Jiming Kang, Po Chen
Department of Geology and Geophysics, University of Wyoming,
Laramie, WY 82071, USA
E-mail: pochengeophysics@gmail.com

Zheming Zhu
College of Architecture and Environment, Sichuan University,
Chengdu, China